**ATLAS Note**

GROUP-2017-XX

1st September 2020

Draft version 0.1

# WZ + Heavy Flavor Production in pp collisions at $\sqrt{s}$ = 13 TeV

## The ATLAS Collaboration

A measurement of WZ produced with an associated heavy flavor jet is performed using 140 fb$^{-1}$ of proton-proton collision data at $\sqrt{s} = 13$ TeV from the ATLAS experiment at the LHC. The measurement is performed in the fully leptonic decay mode, $WZ \rightarrow l\nu ll$. The cross-section of WZ + b-jets is measured to be X ± X ± X, while the cross-section of WZ + charm is measured as X, with a correlation of X between the two processes.

# Contents

# 1 Changes and outstanding items

## 1.1 Changelog

This is version 3

### 1.1.1 Changes relative to v2

- Included a section on tZ interference effects, **??**.
- Updated to reflect changes for 2018, including the move to PFlow jets, DL1r, updated trigger, and updated AnalysisBase version (now 21.2.127)

### 1.1.2 Changes relative to v1

- Added GRL list
- Fixed latex issue in line 92, typo in line 172
- Added tables **??** and **??**, summarizing the event and object selection
- Added table **??**, which includes the DSID of samples used
- Included reference to WZ inclusive paper in introduction

## 1.2 Outstanding Items

- Include new Madgraph WZjj VBS samples - currently using Sherpa, which is missing b-jet diagrams
- Move to updated 2018 data and MC recommendations
- Understand data/MC discrepancies, likely from fake contribution. Possibly move to data driven fakes
- Investigate VVV samples, ensure no overlap with WZjj samples
- Include selection to reject events with a fourth soft lepton to reduce ZZ->llll contribution
- Add details on top mass reconstruction, specifically to justify choices made

## 2 Introduction

The production of $WZ$ in association with a heavy flavor jet represents an important background for many major analyses. This includes any process with leptons and b-jets in the final state, such as $t\bar{t}H$, $t\bar{t}W$, and $t\bar{t}Z$. While precise measurements have been made of $WZ$ production [1], $WZ$ + heavy flavor remains poorly understood. This is largely because the QCD processes involved in the production of the b-jet make it difficult to simulate accurately. This introduces a large uncertainty for analyses that include this process as a background.

Motivated by its relevance to the $t\bar{t}H$ multilepton analysis, we perform a study of the fully leptonic decay mode of this channel; that is, events where both the W and Z decay leptonically. Because WZ has no associated jets at leading order, while the major backgrounds for this channel tend to have high jet multiplicity, events with more than two jets are rejcted. This gives a final state signature of three leptons and one or two jets.

Events that meet this selection criteria are sorted into pseudo-continuous b-tagging regions based on the DL1r b-tag score of their associated jets. This is done to separate $WZ$ + b-jet events from $WZ$ + charm and $WZ$ + light jets. These regions are fit to data in order make a more accurate estimate of the contribution of $WZ$ + heavy-flavor, where heavy-flavor jets include b-jets and charm jets. The full Run-2 dataset collected by the ATLAS detector, representing 139 fb$^{-1}$ of data from pp collisions at $\sqrt{s} = 13$ TeV, is used for this study.

Section **??** details the data and Monte Carlo (MC) samples used in the analysis. The reconstruction of various physics objects is described in section **??**. Section **??** describes the event selection applied to these samples. The multivariate analysis techniques used to separate the tZ background from WZ + heavy flavor are described in section **??**. The regions defined for the fit are then described in section **??**. Section **??** describes the various sources of systematic uncertainties considered in the fit. Finally, the results of the analysis are summarized in section **??**, followed by a brief conclusion in section **??**.

**The current state of the analysis shows blinded results for the full 2018 dataset, awaiting unblinding approval.**

## 3 Data and Monte Carlo Samples

Both data and Monte Carlo samples used in this analysis were prepared in the `xAOD` format, which was used to produce a `DxAOD` sample in the `HIGG8D1` derivation framework. The `HIGG8D1` framework is designed for the $t\bar{t}H$ multi-lepton| analysis, which targets events with multiple leptons as well as tau hadrons. This framework skims the dataset to remove unneeded variables as well as entire events. Events are removed from the derivations that do not meet the following selection:

- at least two light leptons within a range $|\eta|$<2.6, with leading lepton $p_T$ > 15 GeV and subleading lepton $p_T$ > 5 GeV

- at least one light lepton with $p_T$ > 15 GeV within a range $|\eta|$<2.6, and at least two hadronic taus with $p_T$ > 15 GeV.

Samples were then generated from these `HIGG8D1` derivations using a modified version of AnalysisBase version 21.2.127.

## 3.1 Data Samples

The study uses a sample of proton-proton collision data collected by the ATLAS detector from 2015 through 2018 at an energy of $\sqrt{s} = 13$ TeV, which represents an integrated luminosity of 139 fb$^{-1}$. This data set was collected with a bunch crossing rate of 25 ns. All data used in this analysis was verified by data quality checks, having been included in the following Good Run Lists:

- data15_13TeV.periodAllYear_DetStatus-v79-repro20-02_DQDefects-00-02-02 _PHYS_StandardGRL_All_Good_25ns.xml

- data16_13TeV.periodAllYear_DetStatus-v88-pro20-21_DQDefects-00-02-04 _PHYS_StandardGRL_All_Good_25ns.xml

- data17_13TeV.periodAllYear_DetStatus-v97-pro21-13_Unknown_PHYS_StandardGRL _All_Good_25ns_Triggerno17e33prim.xml

- data18_13TeV.periodAllYear_DetStatus-v102-pro22-04_Unknown_PHYS_StandardGRL _All_Good_25ns_Triggerno17e33prim.xml

## 3.2 Monte Carlo Samples

Several different generators were used to produce Monte Carlo simulations of the signal and background processes. For all samples, the response of the ATLAS detector is simulated using Geant4. The WZ signal samples are simulated using Sherpa 2.2.2 [2]. Specific information about the Monte Carlo samples being used can be found in table **??**. A list of the specific samples used by data set ID is shown in table **??**.

Table 1: The configurations used for event generation of signal and background processes, including the event generator, matrix element (ME) order, parton shower algorithm, and parton distribution functin (PDF).

| Process | Event generator | ME order | Parton Shower | PDF |
|---|---|---|---|---|
| $WZ$, $VV$ | Sherpa 2.2.2 | MEPS NLO | Sherpa | CT10 |
| $tZ$ | MG5_aMC | LO | Pythia 6 | CTEQ6L1 |
| $t\bar{t}W$ | MG5_aMC | NLO | Pythia 8 | NNPDF 3.0 NLO |
| | (Sherpa 2.1.1) | (LO multileg) | (Sherpa) | (NNPDF 3.0 NLO) |
| $t\bar{t}(Z/\gamma^* \to ll)$ | MG5_aMC | NLO | Pythia 8 | NNPDF 3.0 NLO |
| $t\bar{t}H$ | MG5_aMC | NLO | Pythia 8 | NNPDF 3.0 NLO [**Ball:2014uwa**] |
| | (MG5_aMC) | (NLO) | (Herwig++) | (CT10 [**ct10**]) |
| $tHqb$ | MG5_aMC | LO | Pythia 8 | CT10 |
| $tHW$ | MG5_aMC | NLO | Herwig++ | CT10 |
| | (Sherpa 2.1.1) | (LO multileg) | (Sherpa) | (NNPDF 3.0 NLO) |
| $tWZ$ | MG5_aMC | NLO | Pythia 8 | NNPDF 2.3 LO |
| $t\bar{t}t$, $t\bar{t}t\bar{t}$ | MG5_aMC | LO | Pythia 8 | NNPDF 2.3 LO |
| $t\bar{t}W^+W^-$ | MG5_aMC | LO | Pythia 8 | NNPDF 2.3 LO |
| $t\bar{t}$ | Powheg-BOX v2 [**powhegtt**] | NLO | Pythia 8 | NNPDF 3.0 NLO |
| $t\bar{t}\gamma$ | MG5_aMC | LO | Pythia 8 | NNPDF 2.3 LO |
| s-, t-channel, | Powheg-BOX v1 [**powhegstp**] | NLO | Pythia 6 | CT10 |
| $Wt$ single top | | | | |
| $qqVV$, $VVV$ | | | | |
| $Z \to l^+l^-$ | Sherpa 2.2.1 | MEPS NLO | Sherpa | NNPDF 3.0 NLO |

# 4 Object Reconstruction

All regions defined in this analysis share a common lepton, jet, and overall event preselection. This preselection is detailed here; the selection used to define the various fit regions is described in section **??**.

## 4.1 Trigger

Events are required to be selected by dilepton triggers, as summarized in table **??**.

## 4.2 Light leptons

Electron candidates are reconstructed from energy clusters in the electromagnetic calorimeter that are associated with charged particle tracks reconstructed in the inner detector [3]. Electron candidates are required to have $p_T > 10$ GeV and $|\eta_{\text{cluster}}| < 2.47$. Candidates in the transition region between different electromagnetic calorimeter components, $1.37 < |\eta_{\text{cluster}}| < 1.52$, are rejected. A multivariate likelihood discriminant combining shower shape and track information is used to distinguish real electrons from hadronic showers (fake electrons). To further reduce

| Sample | DSID |
|---|---|
| WZ | 364253, 364739-42 |
| VV | 364250, 364254, 364255, 363355-60, 364890 |
| t$\bar{\text{t}}$W | 410155 |
| t$\bar{\text{t}}$Z | 410156, 410157, 410218-20 |
| low mass t$\bar{\text{t}}$Z | 410276-8 |
| Rare Top | 410397, 410398, 410399 |
| single Top | 410658-9, 410644-5 |
| three Top | 304014 |
| four Top | 410080 |
| t$\bar{\text{t}}$WW | 410081 |
| Z + jets | 364100-41 |
| low mass Z + jets | 364198-215 |
| W + jets | 364156-97 |
| V$\gamma$ | 364500-35 |
| tZ | 410560 |
| tW | 410013-4 |
| WtZ | 410408 |
| VVV | 364242-9 |
| VH | 342284-5 |
| WtH | 341998 |
| t$\bar{\text{t}}\gamma$ | 410389 |
| t$\bar{\text{t}}$ | 410470 |
| t$\bar{\text{t}}$H | 345873-5, 346343-5 |

Table 2: List of Monte Carlo samples by data set ID used in the analysis.

the non-prompt electron contribution, the track is required to be consistent with originating from the primary vertex; requirements are imposed on the transverse impact parameter significance ($|d_0|/\sigma_{d_0}$) and the longitudinal impact parameter ($|\Delta z_0 \sin \theta_\ell|$), as shown in table **??**.

Muon candidates are reconstructed by combining inner detector tracks with track segments or full tracks in the muon spectrometer [4]. Muon candidates are required to have $p_T > 10$ GeV and $|\eta| < 2.5$.

All leptons are required to be isolated, and pass a non-prompt BDT selection described in detail in [5].

## 4.3 Jets

Jets are reconstructed from calibrated topological clusters built from energy deposits in the calorimeters [6], using the anti-$k_t$ algorithm with a radius parameter $R = 0.4$. Jets with energy contributions likely arising from noise or detector effects are removed from consideration [7],

| Dilepton triggers (2015) | |
|---|---|
| μμ (asymm.) | HLT_mu18_mu8noL1 |
| ee (symm.) | HLT_2e12_lhloose_L12EM10VH |
| eμ, μe (~symm.) | HLT_e17_lhloose_mu14 |
| Dilepton triggers (2016) | |
| μμ (asymm.) | HLT_mu22_mu8noL1 |
| ee (symm.) | HLT_2e17_lhvloose_nod0 |
| eμ, μe (~symm.) | HLT_e17_lhloose_nod0_mu14 |
| Dilepton triggers (2017) | |
| μμ (asymm.) | HLT_mu22_mu8noL1 |
| ee (symm.) | HLT_2e24_lhvloose_nod0 |
| eμ, μe (~symm.) | HLT_e17_lhloose_nod0_mu14 |
| Dilepton triggers (2018) | |
| μμ (asymm.) | HLT_mu22_mu8noL1 |
| ee (symm.) | HLT_2e24_lhvloose_nod0 |
| eμ, μe (~symm.) | HLT_e17_lhloose_nod0_mu14 |

Table 3: List of lowest $p_T$-threshold, un-prescaled dilepton triggers used for 2015-2018 data taking.

and only jets satisfying $p_T > 25$ GeV and $|\eta| < 2.5$ are used in this analysis. For jets with $p_T < 60$ GeV and $|\eta| < 2.4$, a jet-track association algorithm is used to confirm that the jet originates from the selected primary vertex, in order to reject jets arising from pileup collisions [8].

## 4.4 B-tagged Jets

In order to make a measurement of $WZ$ + heavy flavor it is necessary to distinguish these events from $WZ$ + light jets. For this purpose, the DL1r b-tagging algorithm is used to distinguish heavy flavor jets from lighter ones. The DL1r algorithm uses jet kinematics, particularly jet vertex information, as input for a neural network which assigns each jet a score designed to reflect how likely that jet is to have originated from a b-quark.

From the output of the BDT, working points (WPs) are developed based on the efficiency of truth b-jets at particular values of the DL1r algorithm. The working points used in this analysis are summarized in table **??**.

A tighter WP will accept fewer b-jets, but reject a higher fraction of charm and light jets. Generally, analyses that include b-jets will use a fixed working point, for example, requiring that a jet pass the 70% threshold. By instead treating these working point as bins, e.g. events with jets that fall between the 85% and 77% WPs fall into one bin, while events with jets passing the

| | $e$ | | | $\mu$ | | |
|---|---|---|---|---|---|---|
| | L | L* | T | L | L* | T |
| FixedCutLoose | No | Yes | | No | Yes | |
| Non-prompt lepton BDT | No | | Yes | No | | Yes |
| Identification | Loose | | Tight | Loose | | Medium |
| Charge mis-assignment veto | No | | Yes | N/A | | |
| ambiguity bit == 0 | No | | Yes | N/A | | |
| Transverse impact parameter significance $|d_0|/\sigma_{d_0}$ | $< 5$ | | | $< 3$ | | |
| Longitudinal impact parameter $|z_0 \sin\theta|$ | $< 0.5$ mm | | | | | |

Table 4: Loose (L), loose and minimally-isolated (L*), and tight (T) light lepton definitions.
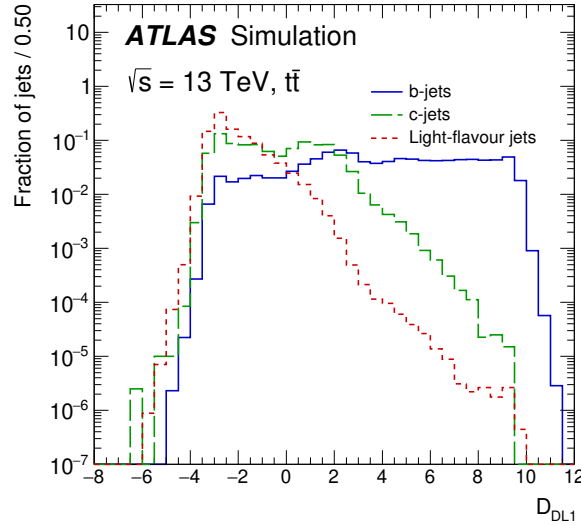


Figure 1: Output distribution of the DL1r algorithm for b-jets, charm jets, and light jets

60% WP fall into another, and looking at the full psuedo-continuous DL1r spectrum of the jets, additional information can be gained. The psuedo-continuous b-tag spectrum is used in this case to separate out WZ + b, WZ + charm, and WZ + light.

## 4.5 Missing transverse energy

Missing transverse momentum ($E_T^{miss}$) is used as part of the event selection. The missing transverse momentum vector is defined as the inverse of the sum of the transverse momenta of

| WP | none | loose | medium | tight | tightest |
|---|---|---|---|---|---|
| b eff. | - | 85% | 77% | 70% | 60% |

Table 5: B-tagging Working Points by tightness and b-jet efficiency

all reconstructed physics objects as well as remaining unclustered energy, the latter of which is estimated from low-$p_T$ tracks associated with the primary vertex but not assigned to a hard object [9].

# 5 Event Selection

Selected events are required to include exactly three reconstructed light leptons passing the requirement described in **??**, which have a total charge of $\pm 1$. As the opposite sign lepton is found to be prompt the vast majority of the time [5], it is required to be loose and isolated, as defined though the standard `isolationFixedCutLoose` working point supported by combined performance groups. The same sign leptons are required to be very tight, as per the recommended `isolationFixedCutTight`.

The leptons are ordered in the analysis code as 0, 1, and 2. Lepton 0 is the lepton whose charge is opposite the other two. Lepton 1 is the lepton closest to the opposite charge lepton, i.e. the smallest $\Delta R$, leaving lepton 2 as the lepton further from the opposite charge lepton. Lepton 0 is required to have $p_T > 10$ GeV, while the same sign leptons, 1 and 2, are required to have $p_T > 20$ GeV to reduce the contribution of non-prompt leptons.

The invariant mass of at least one pair of opposite sign, same flavor leptons is required to fall within 10 GeV of the mass of the Z boson, 91.2 GeV. Events where one of the opposite sign pairs have an invariant mass less than 12 GeV are rejected in order to suppress low mass resonances.

An additional requirement is placed on the missing transverse energy, $E_T^{miss} > 20$ GeV, and the transverse mass of the $W$ candidate, $m(E_T^{miss} + l_{other}) > 30$ GeV, where $E_T^{miss}$ is the missing transverse energy, and $l_{other}$ is the lepton not included in the Z-candidate.

Events are required to have one or two reconstructed jets passing the selection described in section **??**. Events with more than two jets are rejected in order to reduce the contribution of backgrounds such as $t\bar{t}Z$ and $t\bar{t}W$, which tend to have higher jet multiplicity. This selection of summarized in table **??**.

## 5.1 Signal Region Validation

The event yields for both data and Monte Carlo are summarized in table **??**, which shows good agreement between data and Monte Carlo, and demonstrates that this signal region consists primarily of WZ events.

| Event Selection |
| --- |
| Exactly three leptons with charge ±1 |
| Two same-charge leptons with $p_T > 20$ GeV |
| One opposite charge lepton with $p_T > 10$ GeV |
| $m(l^+l^-)$ within 10 GeV of 91.2 GeV |
| Transverse mass of W-candidate, $m_T(E_T^{miss} + lep_{other}) > 30$ GeV |
| Missing transverse energy, $E_T^{miss} > 20$ GeV |
| One or two jets with $p_T > 25$ GeV |

Table 6: Summary of the selection applied to events for inclusion in the fit

| Process | Events |
| --- | --- |
| $WZ + b$ | $167.64 \pm 6.44649$ |
| $WZ + c$ | $1080.91 \pm 39.2803$ |
| $WZ + l$ | $7223.37 \pm 312.532$ |
| Other $VV$ | $849.79 \pm 142.13$ |
| $t\bar{t}W$ | $16.8144 \pm 2.30573$ |
| $t\bar{t}Z$ | $114.679 \pm 17.4006$ |
| $t\bar{t}lllowmass$ | $0.51 \pm 0.06$ |
| rare Top | $2.20 \pm 0.14$ |
| Single top | $0.10 \pm 0.45$ |
| Three top | $0.01 \pm 0.01$ |
| Four top | $0.02 \pm 0.01$ |
| $t\bar{t}WW$ | $0.23 \pm 0.05$ |
| $Z + $ jets | $601.16 \pm 260.13$ |
| $V + \gamma$ | $36.51 \pm 54.34$ |
| $tZ$ | $194.64 \pm 65.74$ |
| $tW$ | $5.49 \pm 1.24$ |
| $WtZ$ | $25.80 \pm 1.07$ |
| $VVV$ | $26.21 \pm 0.87$ |
| $VH$ | $94.34 \pm 7.35$ |
| $t\bar{t}$ | $107.68 \pm 8.14$ |
| $t\bar{t}H$ | $4.28 \pm 0.46$ |
| Total | $10556.8 \pm 533.4$ |
| Data | $10574$ |

Table 7: Events yields in the preselection region at 138.9 fb$^{-1}$

Here Other $VV$ represents diboson processes other than WZ, and consists predominantly of $ZZ \rightarrow llll$ events where one of the leptons is not reconstructed.

Simulations are further validated by comparing the kinematic distributions of the Monte Carlo

174 with data in the preselection region, and each of the fit regions, which are shown in figures
175 **??-??**.

### WZ Fit Region - Inclusive

Figure 2: Comparisons between the data and MC distributions in the preselection region for the $p_T$ of (a) the leading jet, (b) lepton 0, (c) lepton 1, (d) lepton 2, (e) the missing transverse energy, and (f) the invariant mass of lepton 0 and 1.
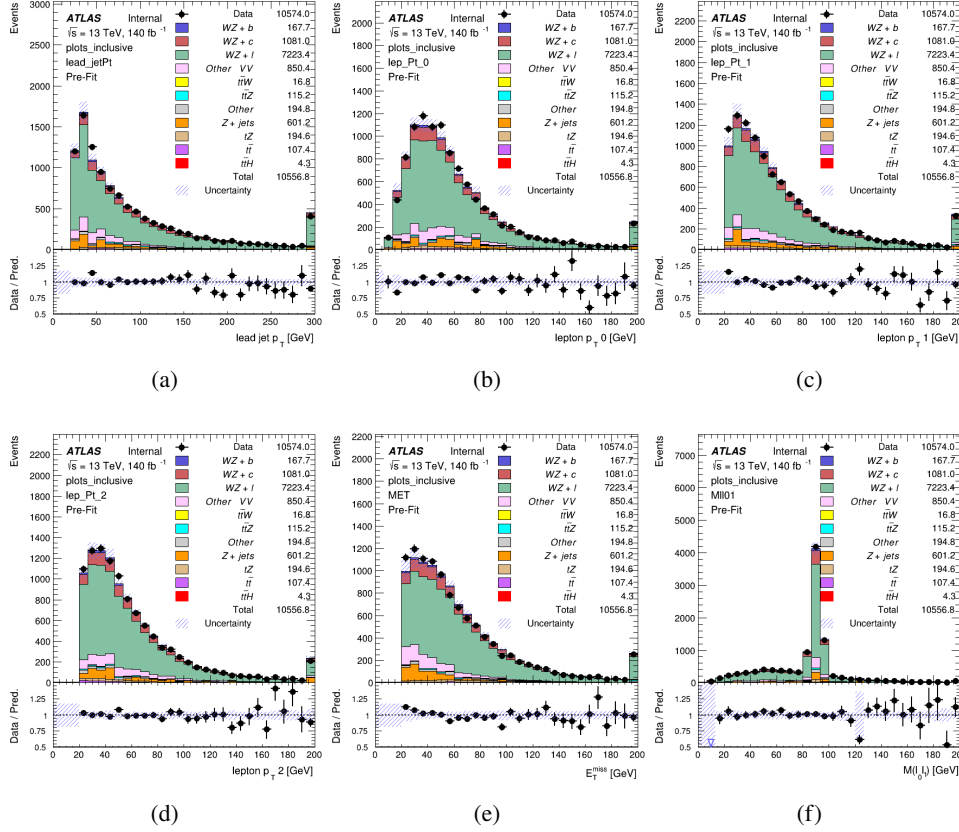


### WZ Fit Region - tZ-CR-2j

## 5.2 Non-Prompt Lepton Estimation

177 Two processes act as sources of non-prompt leptons appear in the analysis: $t\bar{t}$ and Z+jet
178 production both produce two prompt leptons, and each contribute to the signal region when
179 an additional non-prompt lepton appears in the event. The contribution of these processes is
180 estimated with Monte Carlo simulations, which are validated using enriched validation regions.

**WZ Fit Region - 1j < 85% WP**



(g)　　　　　　　　　(h)　　　　　　　　　(i)



(j)　　　　　　　　　(k)　　　　　　　　　(l)
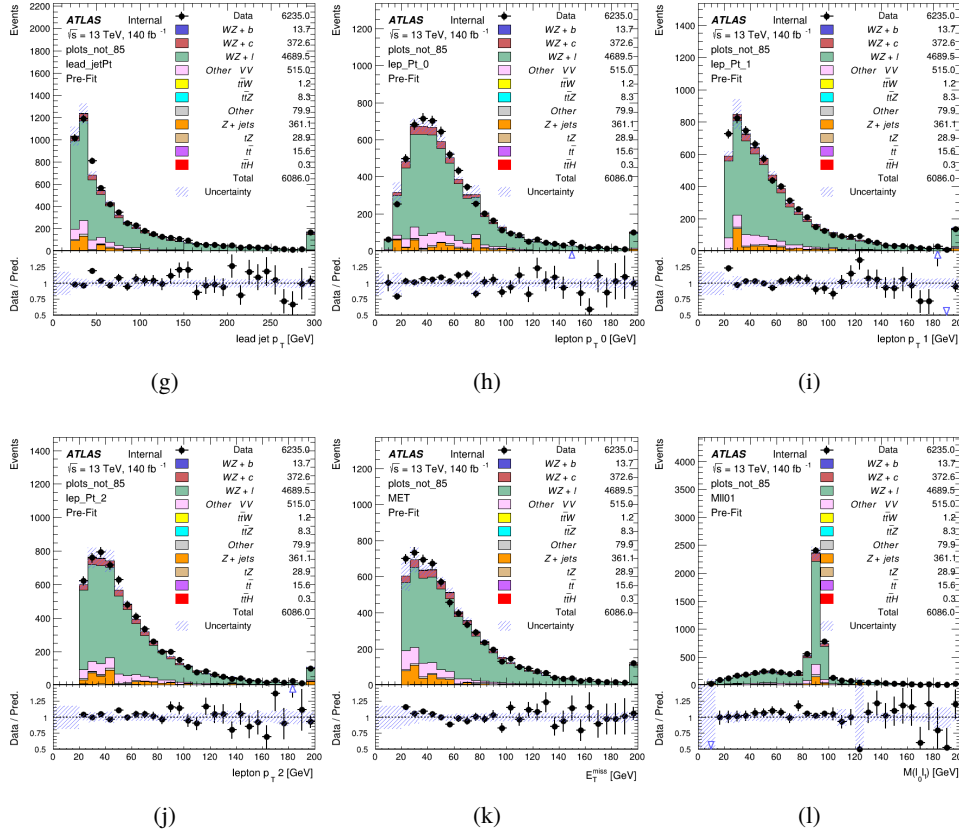
### 5.2.1 $t\bar{t}$ Validation

$t\bar{t}$ events can produce two prompt leptons from the decay of each of the tops. These top decays produce two b-quarks, the decay of which can produce additional non-prompt leptons, which occasionally pass the selection of the signal region. In order to validate that the Monte Carlo accurately simulates this process accurately, the MC prediction in a non-prompt $t\bar{t}$ enriched validation region is compared to data.

The $t\bar{t}$ validation region is similar to the signal region - three leptons meeting the criteria described in section **??** are required, and the requirements on $E_T^{miss}$ remain the same. However, the selection requiring a lepton pair form a Z-candidate are reversed. Events where the invariant mass of any two opposite sign, same flavor leptons falls within 10 GeV of 91.2 GeV are rejected. This ensures the $t\bar{t}$ validation region is orthogonal to the signal region.

Further, because the jet multiplicity of $t\bar{t}$ events tends to be higher than WZ, the number of jets in each event is required to be greater than 1. As b-jets are almost invariably produced from top decays, at least one b-tagged jet in each event is required.
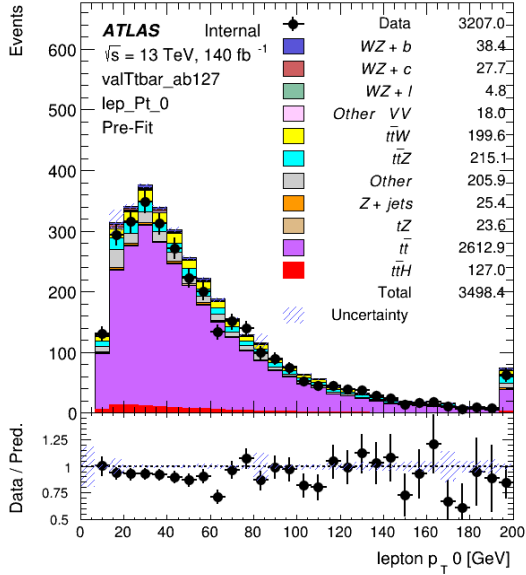
**WZ Fit Region - 1j 77-85% WP**
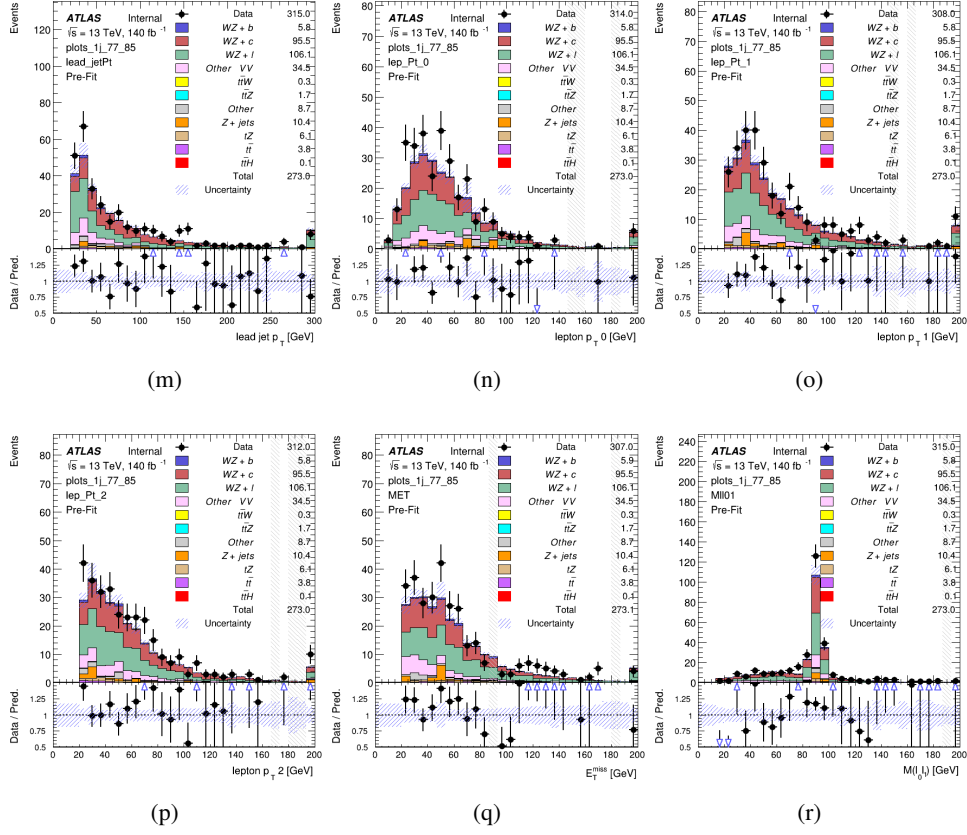
(m)

(n)

(o)

(p)

(q)

(r)
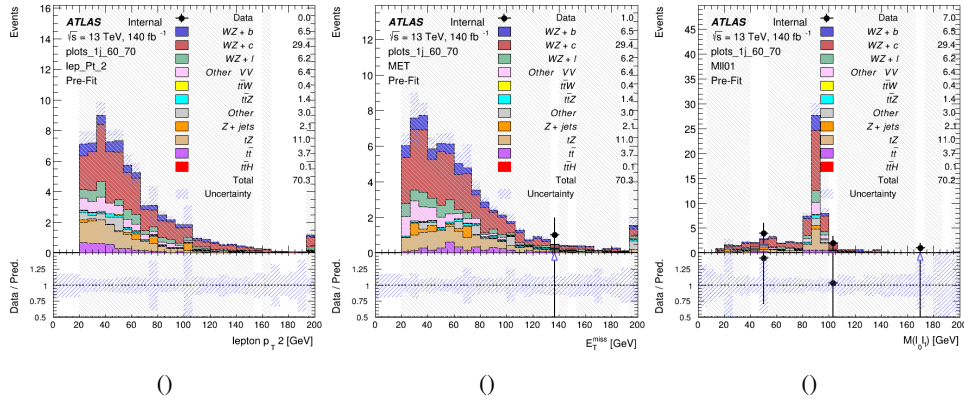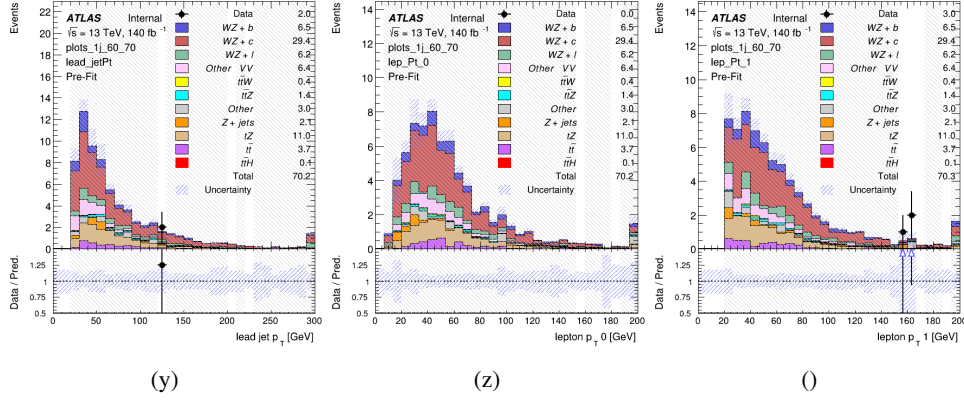
Various kinematic plots of this region are shown below. The general agreement between data and MC in each of these suggests that the non-prompt contribution of $t\bar{t}$ is well modeled by Monte Carlo.

## WZ Fit Region - 1j 70-77% WP



(s)



(t)



(u)



(v)



(w)



(x)



()



()
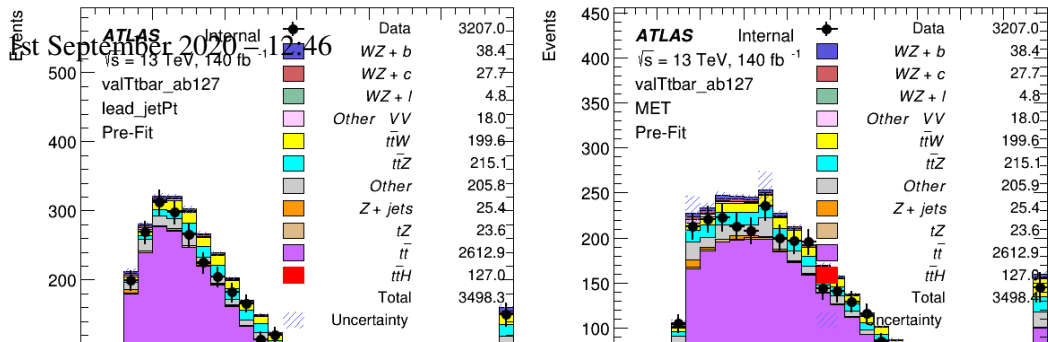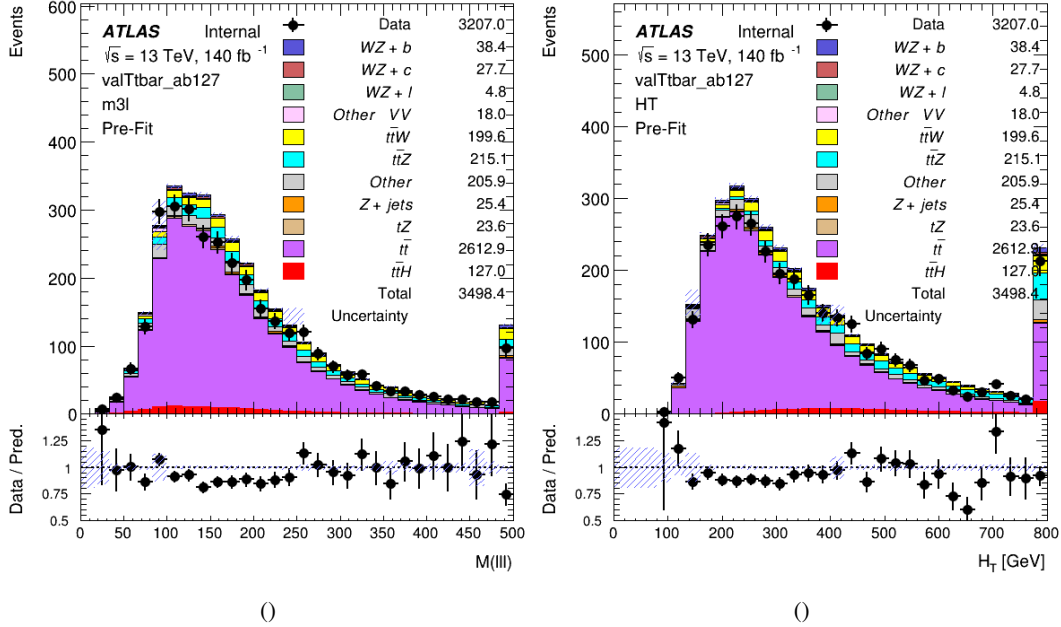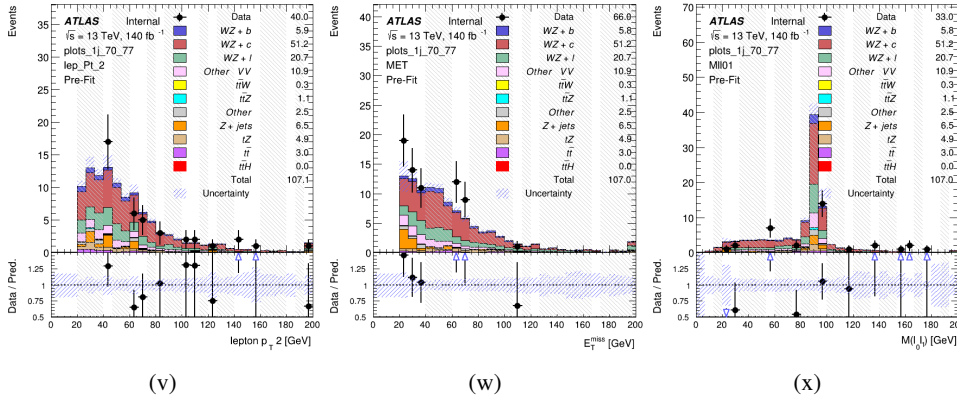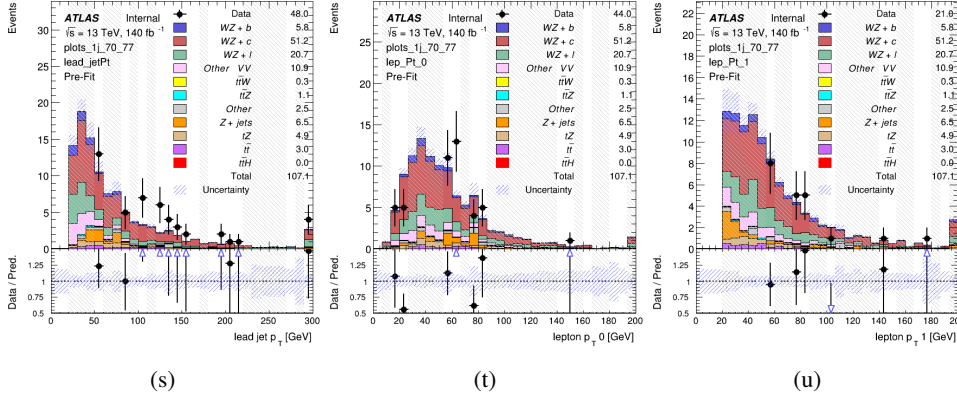
**WZ Fit Region - 1j 60-70% WP**



(y)



(z)



()



()



()



()



(a)



(b)
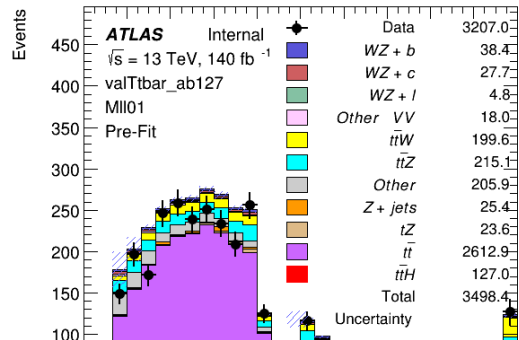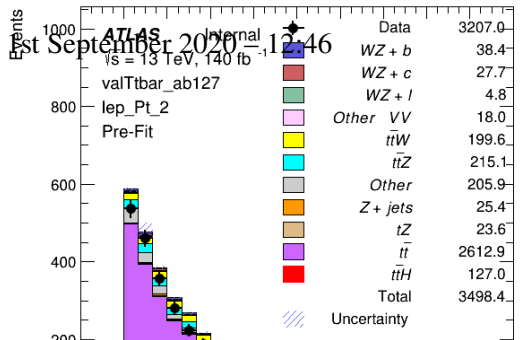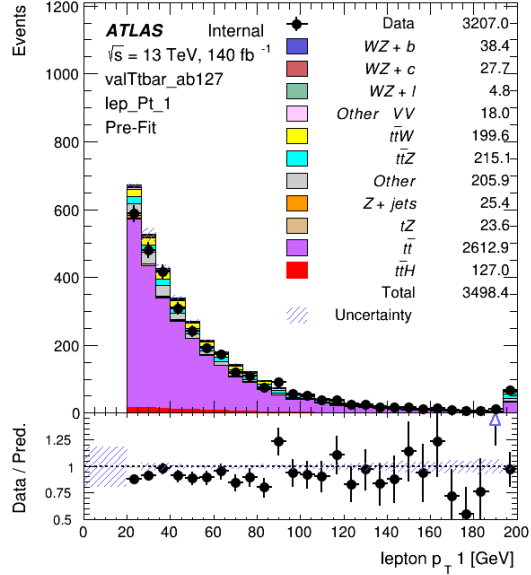
**WZ Fit Region - 1j 60% WP**



()



()



()



()



()



()



(a)



(b)
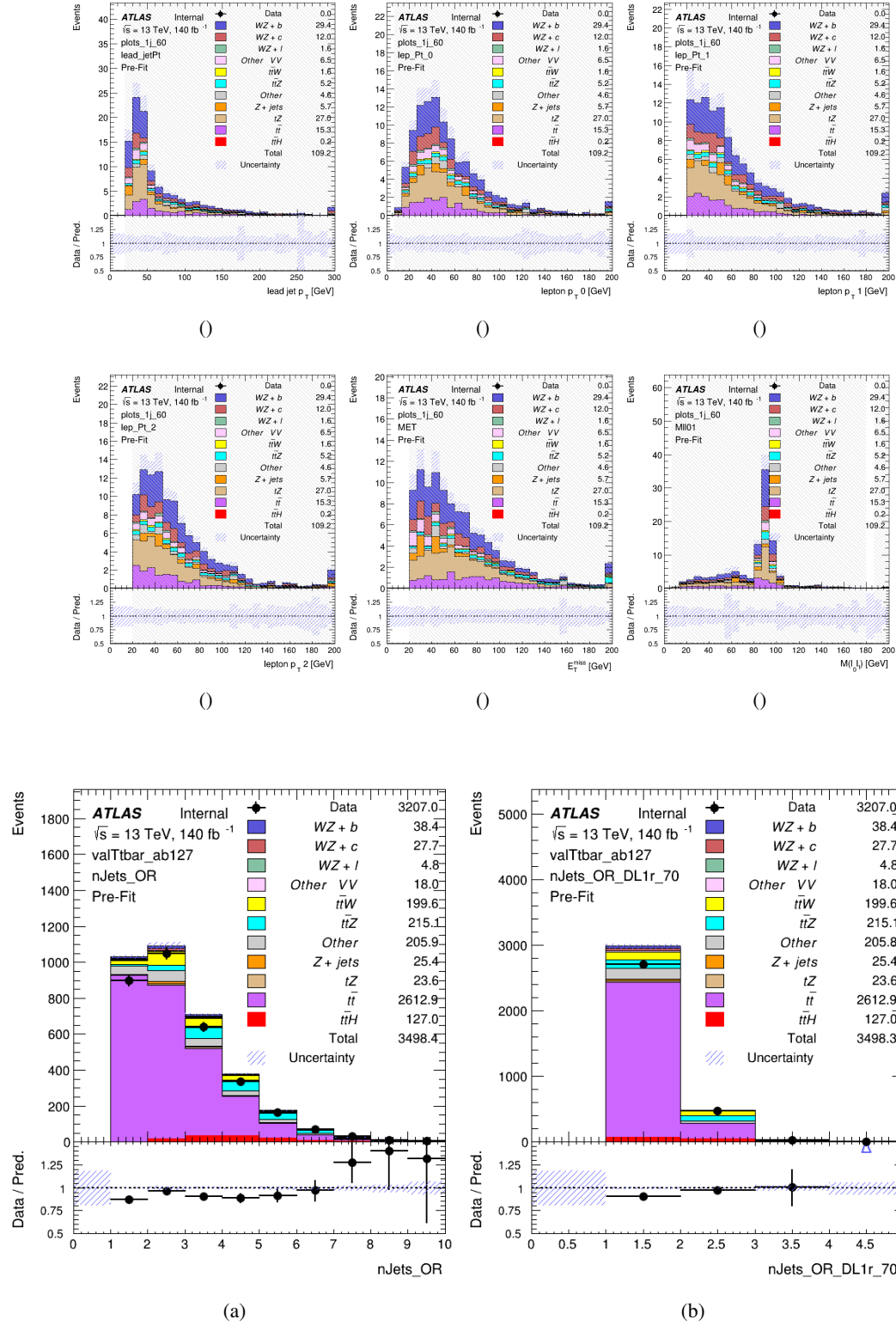
Figure 5: Comparisons between the data and MC distributions in the $t\bar{t}$ validation region for (a) the number of jets (b) the number of b-tagged jets.

**WZ Fit Region - tZ-CR**



()



()



()



()



()



()
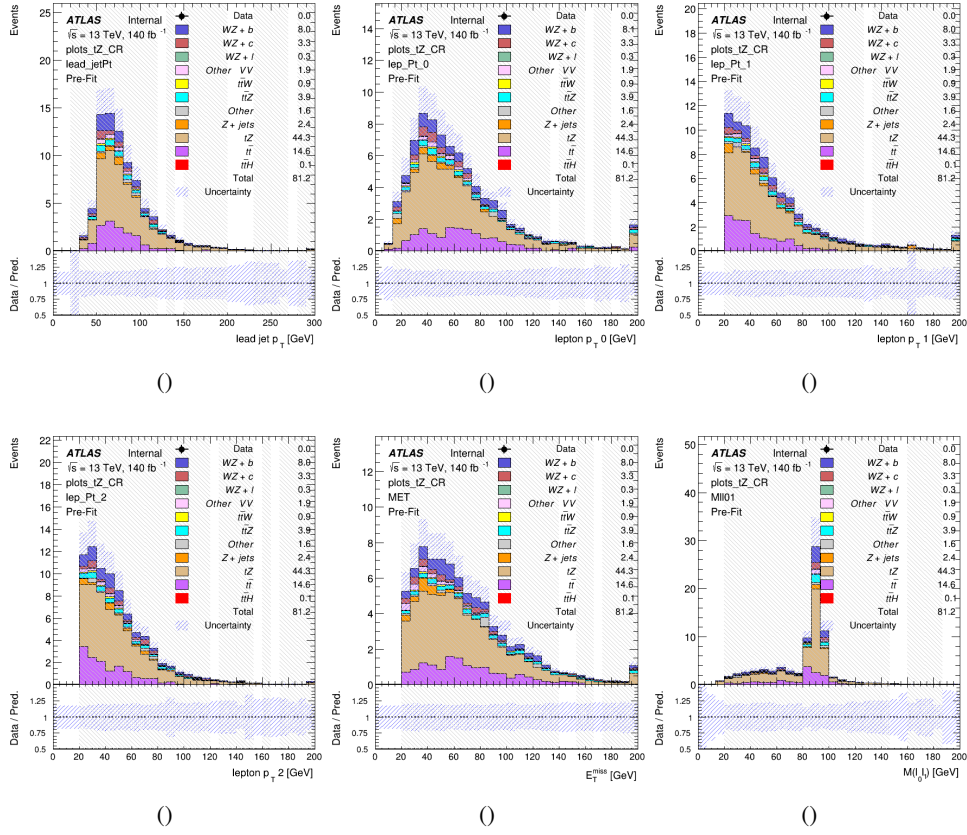
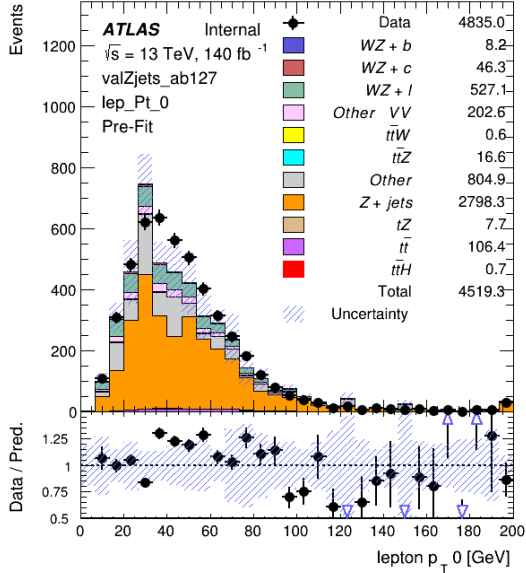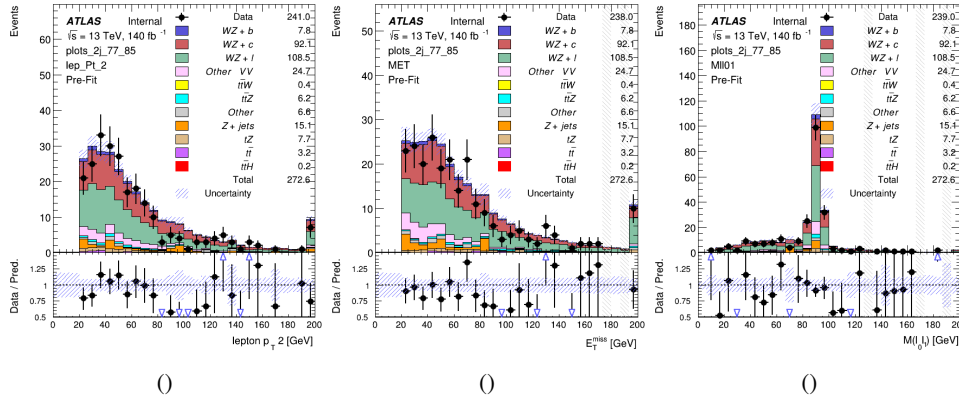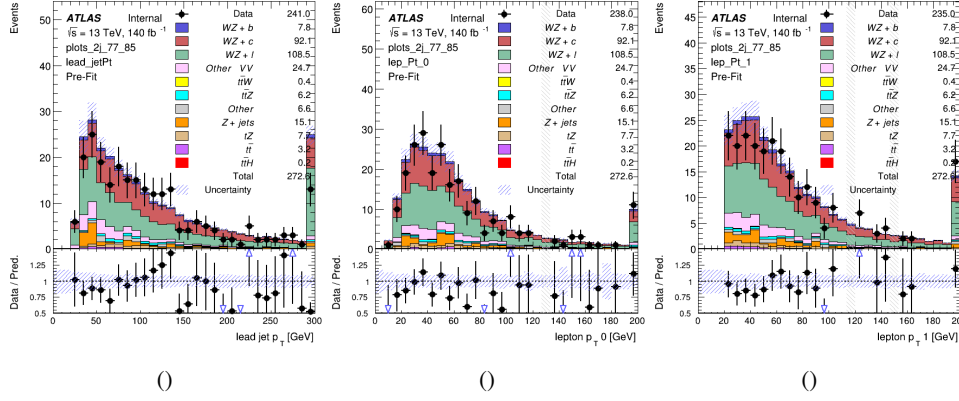### 5.2.2  Z+jets Validation

Similar to $t\bar{t}$, a non-prompt Z+jets validation region is produced in order to validate the MC predictions. The lepton requirements remain the same as the signal region. Because no neutrinos are present for this process, the $E_T^{miss}$ cut is reversed, requiring $E_T^{miss} < 30$ GeV. This also ensures this validation region is orthogonal to the signal region. Further, the number of jets in each event is required to be greater than one.
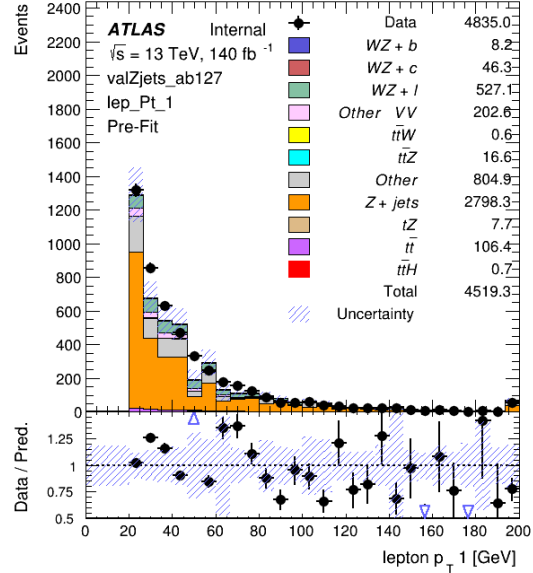
Various kinematic plots of this region are shown below. The general agreement between data and MC in each of these suggests that the non-prompt contribution of Z+jets is well modeled by Monte Carlo.

## WZ Fit Region - 2j < 85% WP



()  ()  ()



()  ()  ()



(a)  (b)
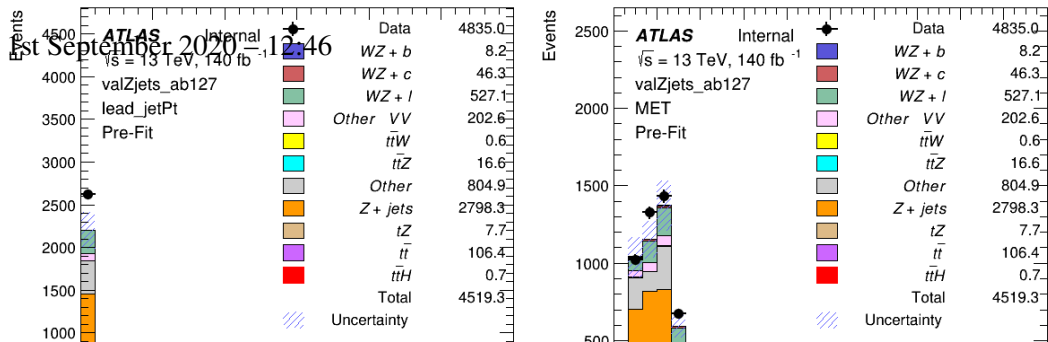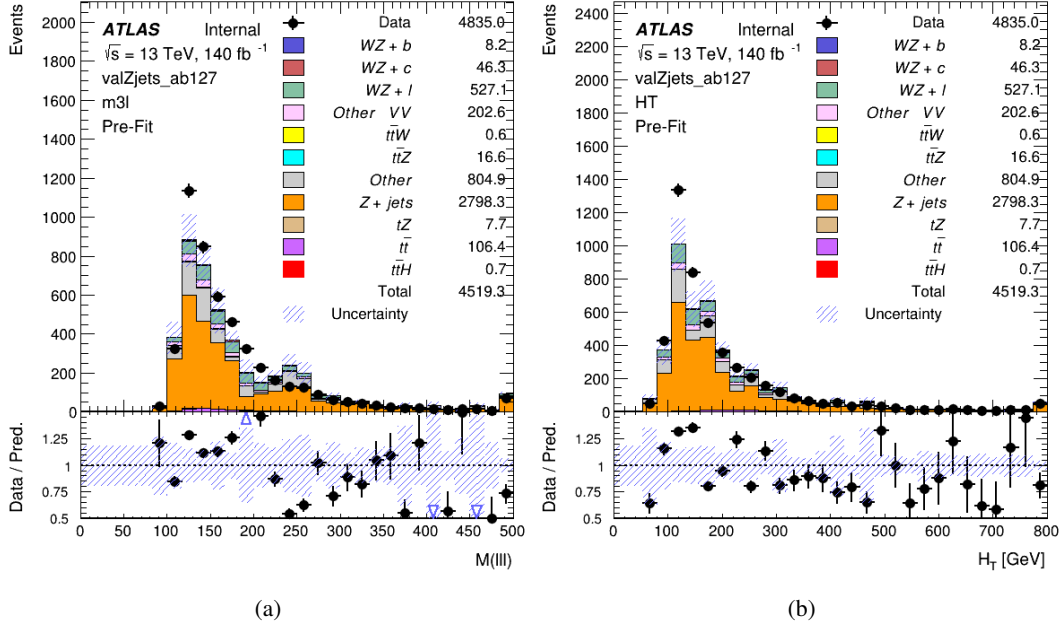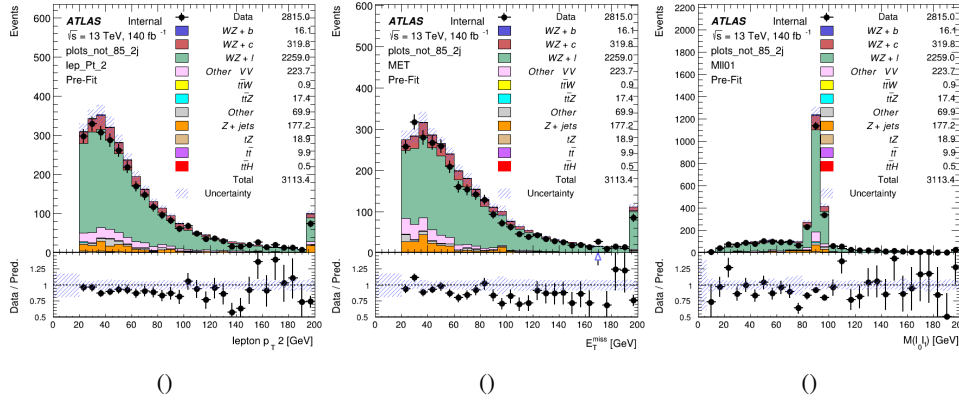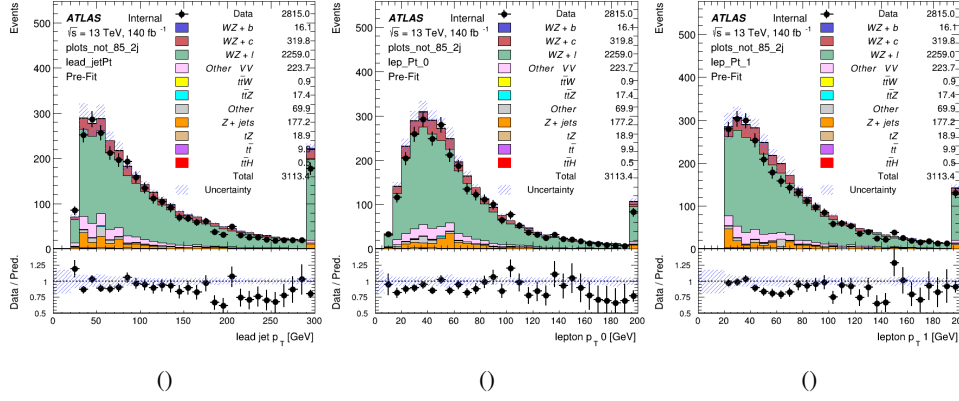
## WZ Fit Region - 2j 77-85% WP



()



()



()



()



()



()



(a)



(b)
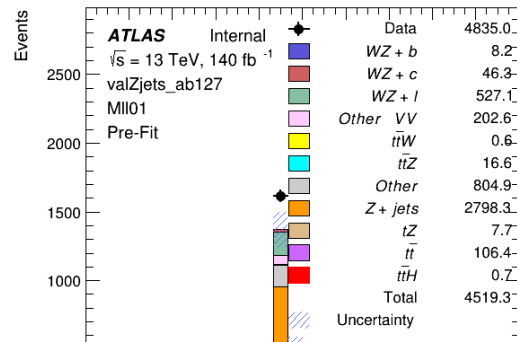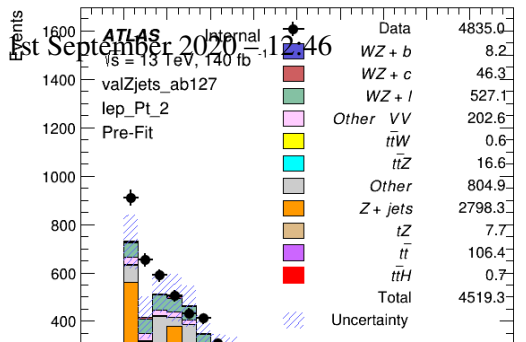
**WZ Fit Region - 2j 70-77% WP**



()



()



()



()



()



()



(a)



(b)
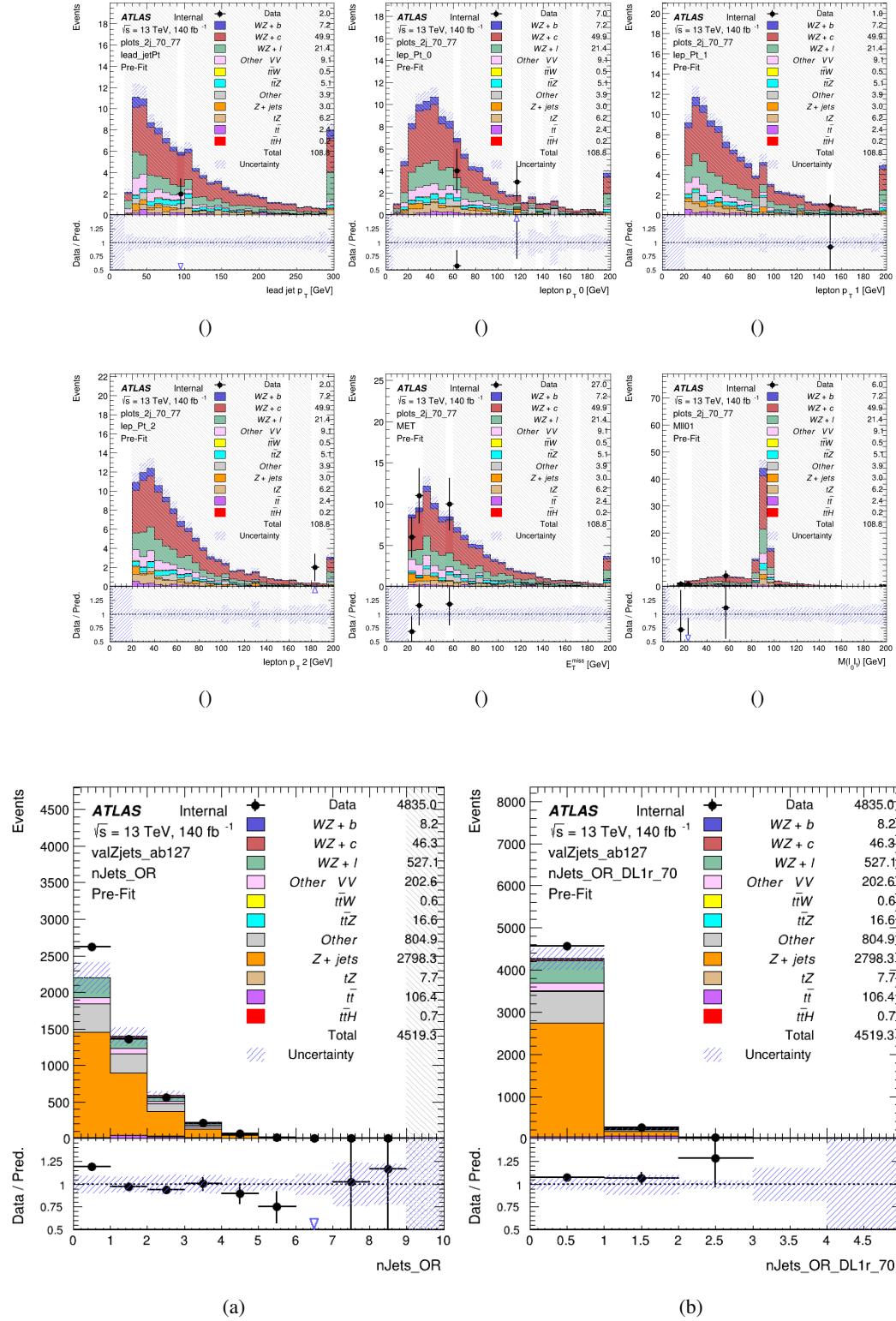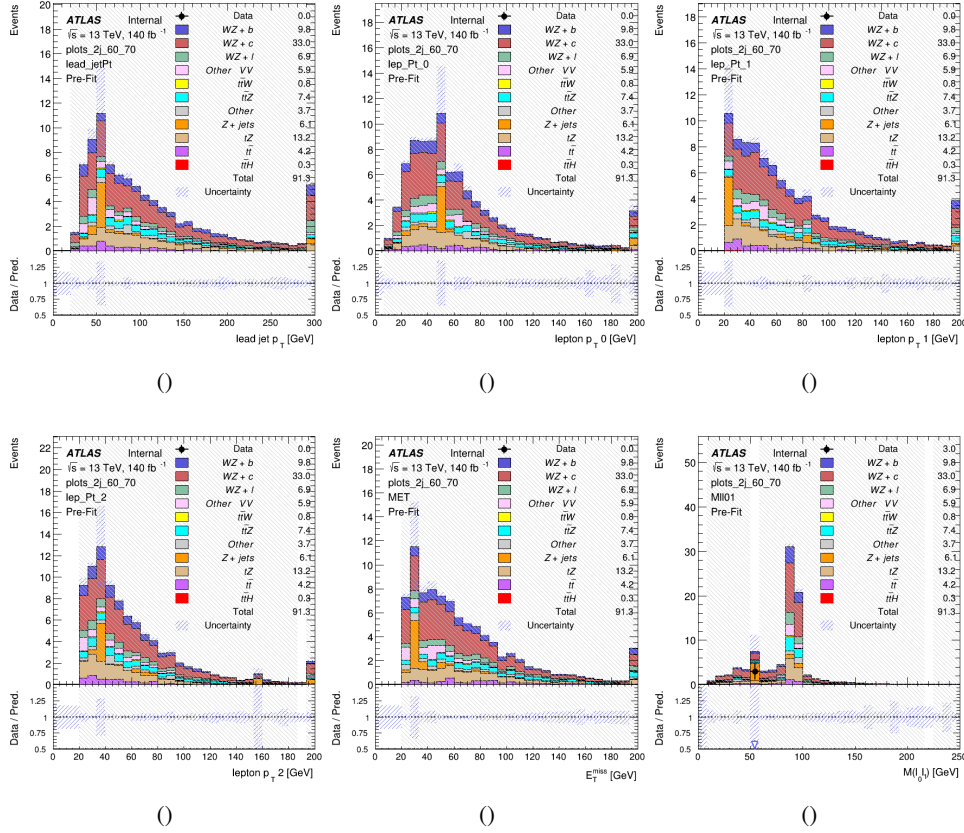
Figure 8: Comparisons between the data and MC distributions in the Z+jets validation region for (a) the number of jets and (b) the number of b-tagged jets.

**WZ Fit Region - 2j 60-70% WP**



()



()



()



()



()



()

## 6 tZ Interference Studies and Separation Multivariate Analysis

Because it includes an on-shell Z boson as well as a b-jet and W from the top decay, tZ production represents an identical final state to WZ + b-jet. This implies the possibility of matrix level interference between these two processes not accounted for in the Monte Carlo simulations, which consider the two processes independently. Truth level studies are performed in order to estimate the impact of these interference effects.

Because tZ produces a final state identical to signal, it represents a predominant background in the most signal enriched regions. Therefore, a boosted decision tree (BDT) algorithm is trained using TMVA [10] to separate $WZ$ + heavy flavor from tZ.

Separation between tZ and $WZ$ + heavy flavor is achieved in part by reconstructing the invariant mass of the top candidate, which clusters more closely to the top mass for tZ than WZ + heavy flavor.

The result of this BDT is used to create a tZ enriched region in the fit, reducing its impact on the measurement of WZ + heavy flavor.

**WZ Fit Region - 2j 60% WP**



()



()



()



()



()



()
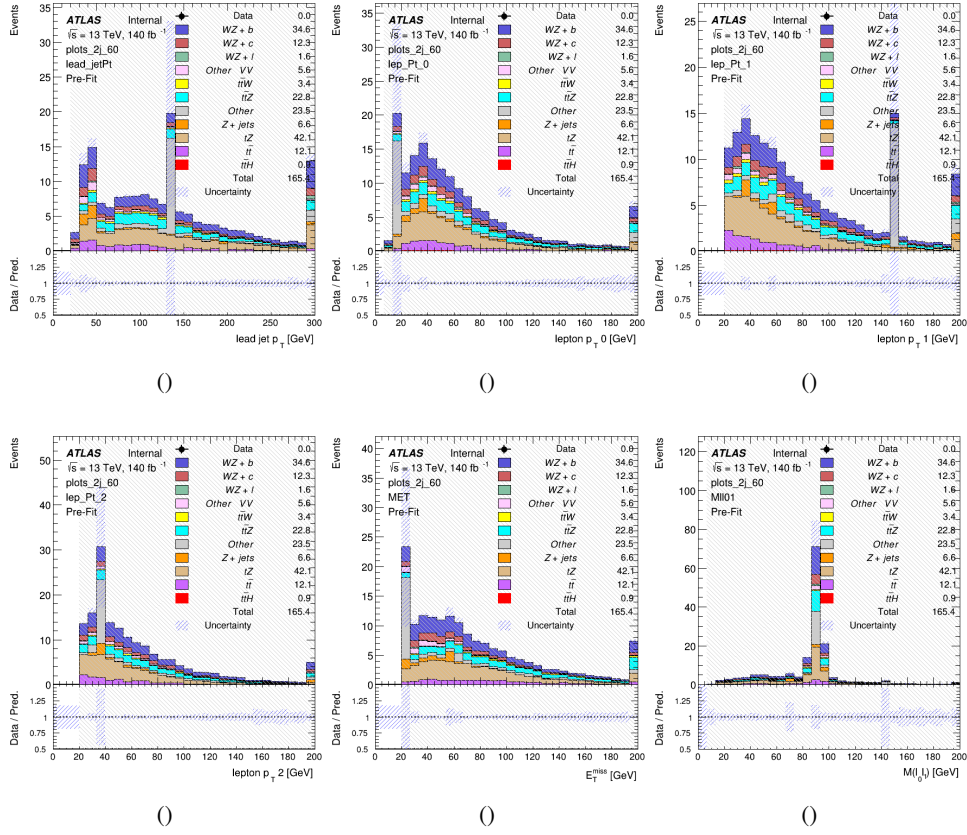
## 6.1 Interference Studies

In order to estimate the matrix level interference effects between tZ and WZ + b-jet, two different sets of simulations are produced using MadGraph 5 [**Madgraph**] - one which simulates these two processes independently, and another where they are produced simultaneously, such that interference effects are present. These two sets of samples are then compared, and the difference between them can be taken to represent any interference effects.

MadGraph simulations of 10,000 tZ and 10,000 WZ + b-jet events are produced, along with 20,000 events where both are present, in the fiducial region where three leptons and at least one jet are produced.

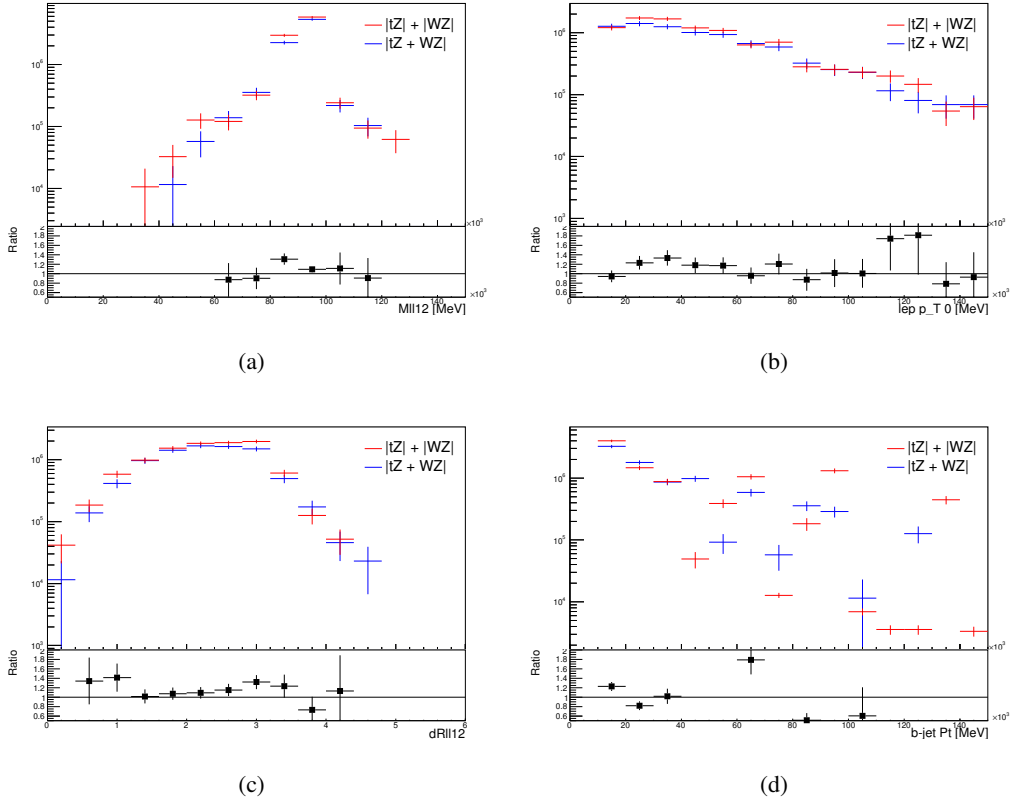The kinematics of these samples are shown below:

(a)

(b)

(c)

(d)

Figure 9: Comparisons between (a) the invariant mass of the Z-candidate, (b) the $p_T$ of the leading lepton, (c) $\Delta(R)$ of the two leptons that form the Z-candidate, and (d) the $p_T$ of the b-jet, for WZ and tZ events generated with interference effects (blue) and without interference effects (red).

## 6.2 Top Mass Reconstruction

The reconstruction of the top mass follows the procedure described in detail in section 6.1 of [11]. The mass of the top quark candidate is reconstructed from the jet, the lepton not included in the Z-candidate, and a reconstructed neutrino. Since the selection requires exactly one jet in the event, there is only possible b-jet candidate.

The neutrino from the W decay is expected to be the only source of $E_T^{miss}$. Therefore, the $E_T$ and $\phi$ of the neutrino are taken from the $E_T^{miss}$ measurement. This leaves the z-component of the neutrino momentum, $p_{vz}$ as the only unknown.

This unknown is solved for by taking the combined invariant mass of the lepton and neutrino to give the invariant mass of the $W$ boson:
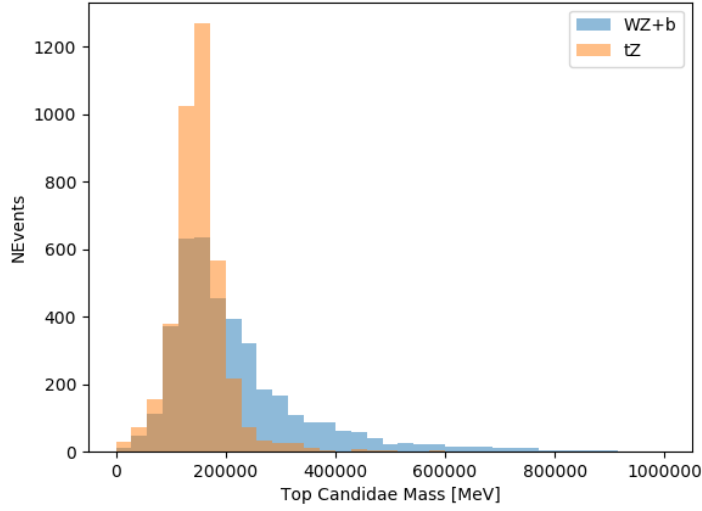
$$(p_l + p_v)^2 = m_W^2$$

Figure 10: Reconstructed top mass distributions for tZ and $WZ + b$, measured in MeV.

Expanding this out into components, this equation gives:

$$\sqrt{p_{T\nu^2} + p_{z\nu^2}}E_l = \frac{m_w^2 - m_l^2}{2} + p_{T\nu}(p_{lx}\cos\phi_\nu + p_{ly}\sin\phi_\nu) + p_{lz}p_{\nu z}$$

This equation gives two solutions for $p_{\nu z}$. For cases where only one of these solutions is real, that is taken as the value of $p_{\nu z}$. For instances with two real solutions, the one which is shown to be correct in the largest fraction of simulations is taken. For cases when no real solution is found, often because of detector effects, the value of $E_T^{miss}$ is varied in decreasing increments of 100 MeV until a real solution is found.

The reconstructed top mass distribution for tZ and $WZ + b$ can be seen in figure **??**.

## 6.3 tZ BDT

The following kinematic variables are used as inputs in order to distinguish between these two processes:

- The invariant mass of the reconstructed top candidate

- $p_T$ of each of the leptons

- $E_T^{miss}$

- Distance between each combination of leptons, $\Delta R(ll)$

257    • Distance between each lepton and the jet, $\Delta R(lj)$

258  The training samples included only events meeting the requirements of the 1-jet, >60% region,
259  i.e. passing all the selection described in section **??** and having exactly one jet which passes the
260  tightest (60%) DL1r working point.

261  The distributions of these features for both signal and background is shown in figure **??**.
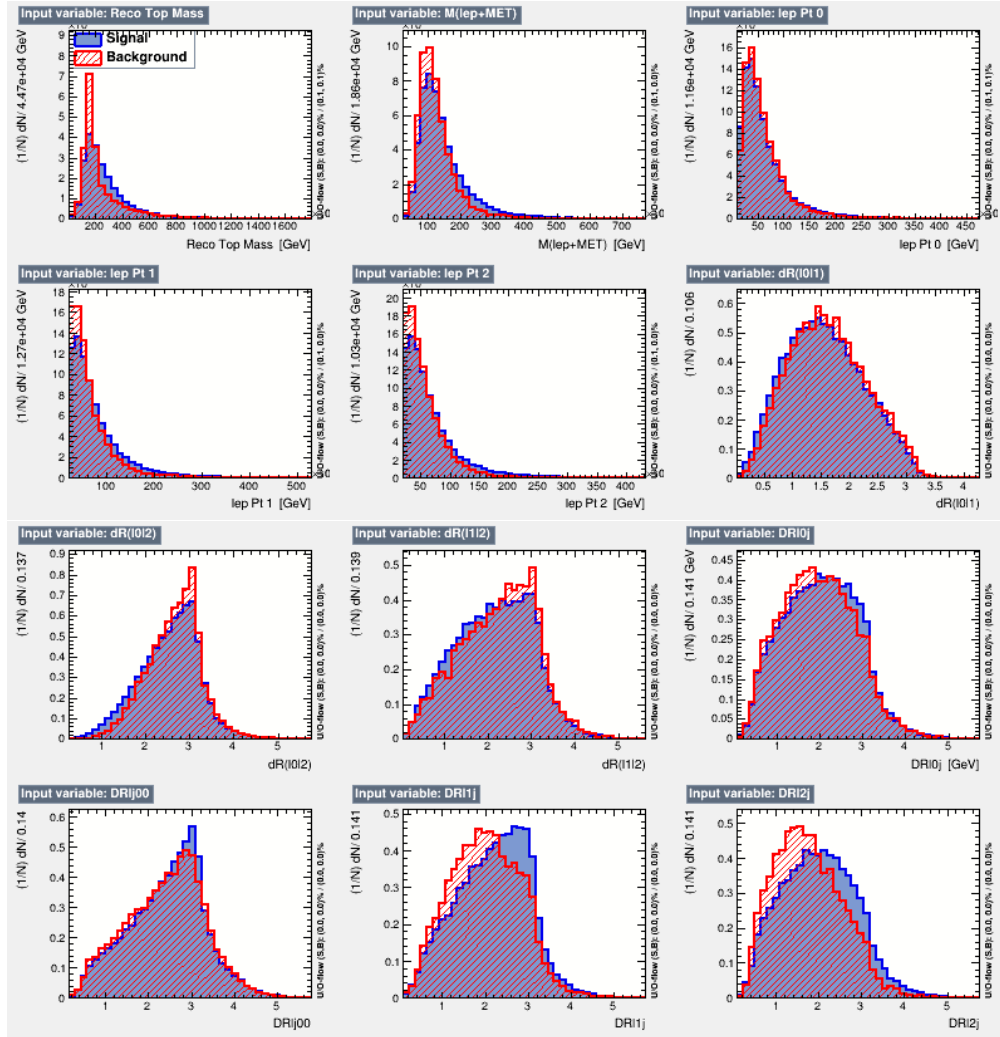


Figure 11: Distribution of input features of the BDT for signal (WZ) and background (tZ).

262  A sample of 20,000 background (tZ) and signal (WZ+b) Monte Carlo events are used to train
263  the BDT. And additional 5,000 events are reserved for testing the model, in order to prevent
264  over-fitting. A total of 750 decision trees with a maximum depth of 6 branches are used to build

265 the model. These parameters are chosen empirically, by training several models with different
266 parameters and selecting the one that gave the best separation for the test sample.

267 The results of the BDT training are shown in figure **??**. The output scores for both signal and
268 background events is shown on the left. The right shows the receiving operating characteristic
269 (ROC) curve that results from the MVA. The ROC curve represents the background rejection
270 as a function of signal efficiency, where each point on the curve represents a different response
271 score. The ROC curve of the BDT is compared to the performance of using an optimal set of flat
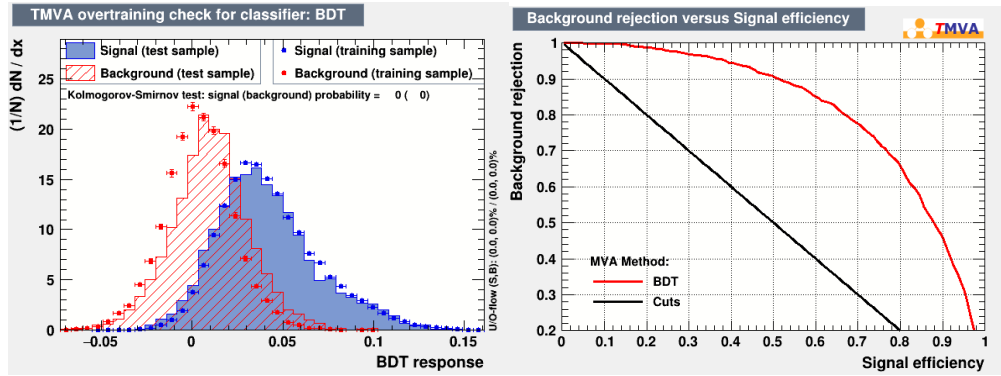272 selections on the same set of input variables.



Figure 12: Distribution of the BDT response for signal and background events on the left, the ROC curve
for the BDT on the right.

273 These results suggest that some amount of separation can be achieved between these two pro-
274 cesses, with a high BDT score selecting a set of events that is pure in $WZ + b$. Further, the ROC
275 curve demonstrates the BDT performs significantly better than a flat selection.

# 7 Signal Region Definitions

277 The regions used in the fit are summarized in table **??**.

278 The working points discussed in section **??** are used to separate events into fit regions based on
279 the highest working point reached by a jet in each event. Because the background composition
280 differs significantly based on the number of b-jets, events are further subdivided into 1 jet and 2
281 jet regions in order to minimize the impact of background uncertainties.

282 An additional tZ control region is created based on the BDT described in section **??**. The region
283 with 1-jet passing the 60% working point is split in two - a signal enriched region of events with
284 a BDT score greater than 0.03, and a tZ control region including events with less than 0.03. This
285 cutoff is arrived at by performing an Asimov fit with a variety of cutoffs, and selecting the value
286 that produces the highest significance for the measurement of $WZ + b$.

Table 8: A list of the regions used in the fit and the selection used for each.

| Region | Selection |
|--------|-----------|
| 1j, <85% | $N_{jets}$ = 1, jet DL1r score < 85% WP |
| 1j, 85%-77% | $N_{jets}$ = 1, 85% < jet DL1r score < 77% WP |
| 1j, 77%-70% | $N_{jets}$ = 1, 77% < jet DL1r score < 70% WP |
| 1j, 70%-60% | $N_{jets}$ = 1, 70% < jet DL1r score < 60% WP |
| 1j, >60% | $N_{jets}$ = 1, jet DL1r score > 85% WP, tZ BDT score > 0.03 |
| 1j tZ CR | $N_{jets}$ = 1, jet DL1r > 85% WP, tZ BDT score < 0.03 |
| 2j, <85% | $N_{jets}$ = 2, jet DL1r score < 85% WP |
| 2j, 85%-77% | $N_{jets}$ = 2, 85% WP < jet DL1r score < 77% WP |
| 2j, 77%-70% | $N_{jets}$ = 2, 77% WP < jet DL1r score < 70% WP |
| 2j, 70%-60% | $N_{jets}$ = 2, 70% < jet DL1r score < 60% WP |
| 2j, >60% | $N_{jets}$ = 2, jet DL1r score > 85% WP, tZ BDT score > 0.03 |
| 2j tZ CR | $N_{jets}$ = 2, jet DL1r score > 85% WP, tZ BDT score < 0.03 |

# 8 Systematic Uncertainties

The systematic uncertainties that are considered are summarized in table **??**. These are implemented in the fit either as a normalization factors or as a shape variation or both in the signal and background estimations. The numerical impact of each of these uncertainties is outlined in section **??**.

The uncertainty in the combined integrated luminosity is derived from a calibration of the luminosity scale performed in August 2015 and May 2016 [12].

The experimental uncertainties are related to the reconstruction and identification of light leptons and b-tagging of jets, and to the reconstruction of $E_T^{miss}$. The sources which contribute to the uncertainty in the jet energy scale [13] are decomposed into uncorrelated components and treated as independent sources in the analysis.

The uncertainties in the b-tagging efficiencies measured in dedicated calibration analyses [14] are also decomposed into uncorrelated components. The large number of components for b-tagging is due to the calibration of the distribution of the MVA discriminant.

The systematic uncertainties associated with the signal and background processes are accounted for by varying the cross-section of each process within its uncertainty.

The full list of systematic uncertainties considered in the analysis is summarized in tables **??**, **??** and **??**.

Table 9: Sources of systematic uncertainty considered in the analysis.

| Systematic uncertainty | Components |
|---|---|
| Luminosity | 1 |
| Pileup reweighting | 1 |
| **Physics Objects** | |
| Electron | 6 |
| Muon | 15 |
| Jet energy scale and resolution | 28 |
| Jet vertex fraction | 1 |
| Jet flavor tagging | 131 |
| $E_T^{miss}$ | 3 |
| Total (Experimental) | 186 |
| **Background Modeling** | |
| Cross section | 24 |
| Renormalization and factorization scales | 10 |
| Parton shower and hadronization model | 2 |
| Shower tune | 4 |
| Total (Signal and background modeling) | 40 |
| Total (Overall) | 226 |

| **Experimental Systematics on Leptons and $E_T^{miss}$** | | | |
|---|---|---|---|
| Type | Description | Systematics Name | Application |
| **Trigger** | | | |
| Scale Factors | Trigger Efficiency | lepSFTrigTight_MU(EL)_SF_Trigger_STAT(SYST) | Event Weight |
| **Muons** | | | |
| Efficiencies | Reconstruction and Identification | lepSFObjTight_MU_SF_ID_STAT(SYST) | Event Weight |
| | Isolation | lepSFObjTight_MU_SF_Isol_STAT(SYST) | Event Weight |
| | Track To Vertex Association | lepSFObjTight_MU_SF_TTVA_STAT(SYST ) | Event Weight |
| $p_T$ Scale | $p_T$ Scale | MUONS_SCALE | $p_T$ Correction |
| Resolution | Inner Detector Energy Resolution | MUONS_ID | $p_T$ Correction |
| | Muon Spectrometer Energy Resolution | MUONS_MS | $p_T$ Correction |
| **Electrons** | | | |
| Efficiencies | Reconstruction | lepSFObjTight_EL_SF_ID | Event Weight |
| | Identification | lepSFObjTight_EL_SF_Reco | Event Weight |
| | Isolation | lepSFObjTight_EL_SF_Isol | Event Weight |
| Scale Factor | Energy Scale | EG_SCALE_ALL | Energy Correction |
| Resolution | Energy Resolution | EG_RESOLUTION_ALL | Energy Correction |
| **$E_T^{miss}$** | | | |
| Soft Tracks Terms | Resolution | MET_SoftTrk_ResoPerp | $p_T$ Correction |
| | Resolution | MET_SoftTrk_ResoPara | $p_T$ Correction |
| | Scale | MET_SoftTrk_ScaleUp | $p_T$ Correction |
| | Scale | MET_SoftTrk_ScaleDown | $p_T$ Correction |

Table 10: Summary of experimental systematics considered for leptons and $E_T^{miss}$. Includes type, description, name of systematic as used in the fit, and mode of application. The mode of application indicates the systematic evaluation, e.g. as an overall event re-weighting (Event Weight) or rescaling ($p_T$ Correction).

| Experimental Systematics on Jets | | | |
|---|---|---|---|
| Type | Origin | Systematics Name | Application |
| Jet Vertex Tagger | | JVT | Event Weight |
| Energy Scale | Calibration Method | JET_21NP_ | $p_T$ Correction |
| | | JET_EffectiveNP_1-19 | $p_T$ Correction |
| | $\eta$ inter-calibration | JET_EtaIntercalibration_Modelling | $p_T$ Correction |
| | | JET_EtaIntercalibration_NonClosure | $p_T$ Correction |
| | | JET_EtaIntercalibration_TotalStat | $p_T$ Correction |
| | High $p_T$ jets | JET_SingleParticle_HighPt | $p_T$ Correction |
| | Pile-Up | JET_Pileup_OffsetNPV | $p_T$ Correction |
| | | JET_Pileup_OffsetMu | $p_T$ Correction |
| | | JET_Pileup_PtTerm | $p_T$ Correction |
| | | JET_Pileup_RhoTopology | $p_T$ Correction |
| | Non Closure | JET_PunchThrough_MC15 | $p_T$ Correction |
| | Flavour | JET_Flavor_Response | $p_T$ Correction |
| | | JET_BJES_Response | $p_T$ Correction |
| | | JET_Flavor_Composition | $p_T$ Correction |
| Resolution | | JET_JER_SINGLE_NP | Event Weight |

Table 11: Jet systematics take into account effects of jets calibration method, $\eta$ inter-calibration, high $p_T$ jets, pile-up, and flavor response. They are all diagonalised into effective parameters.

| Experimental Systematics on b-tagging | | |
|---|---|---|
| Type | Origin | Systematic Name |
| Scale Factors | DL1r b-tagger efficiency on b originated jets in bins of η | DL1r_Continuous_EventWeight_B0-29 |
| | DL1r b-tagger efficiency on c originated jets in bins of η | DL1r_Continuous_EventWeight_C0-19 |
| | DL1r b-tagger efficiency on light flavoured originated jets in bins of η and $p_T$ | DL1r_Continuous_EventWeight_Light0-79 |
| | DL1r b-tagger extrapolation efficiency | DL1r_Continuous_EventWeight_extrapolation DL1r_Continuous_EventWeight_extrapolation_from_charm |

Table 12: Summary of experimental systematics to be included for b-tagging of jets in the analysis, using the continuous DL1r tagging algorithm. All of the b-tagging related systematics are applied as event weights. From left: type, description, and the name of systematic used in the fit.

# 9 Results

A maximum-likelihood fit is performed simultaneously over these nine regions in order to extract the best-fit value of the WZ + b-jet and WZ + charm jet contributions. The $WZ$ + b, $WZ$ + charm and $WZ$ + light contributions are allowed to float, with the remaining background contributions are held fixed. **The current fit strategy treats the WZ + b-jet contribution as the parameter of interest, with the normalization of the $WZ$ + charm and the $WZ$ + light contributions taken as systematic uncertainties. This could however be adjusted, depending on whether it is decided the goal of the analysis should be to measure WZ+b specifically or WZ + heavy flavor overall.** The result of the fit is used to extract the cross-section of $WZ$ + heavy-flavor production.

A maximum likelihood fit to data is performed simultaneously in the eight regions described in section **??**. The parameters $\mu_{WZ+b}$, $\mu_{WZ+charm}$, $\mu_{WZ+light}$, where $\mu = \sigma_{observed}/\sigma_{SM}$, are extracted from the fit.

**The results of the fit are currently blinded.** The post-fit yields in each region are summarized in figure **??**.

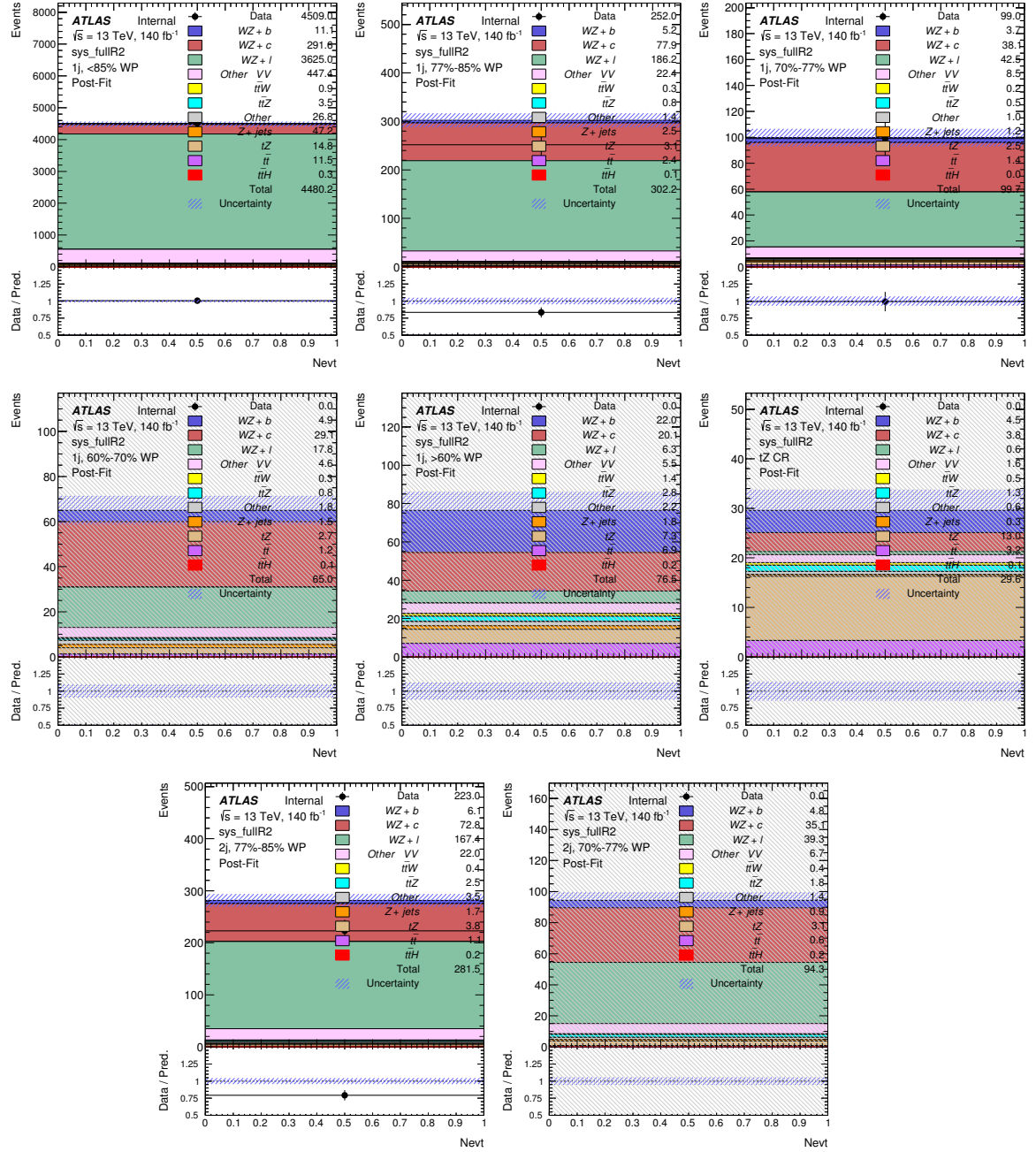A post-fit summary plot of the fitted regions is shown in figure **??**:

Figure 13: Data/MC results in each of the regions after the fit has been performed.
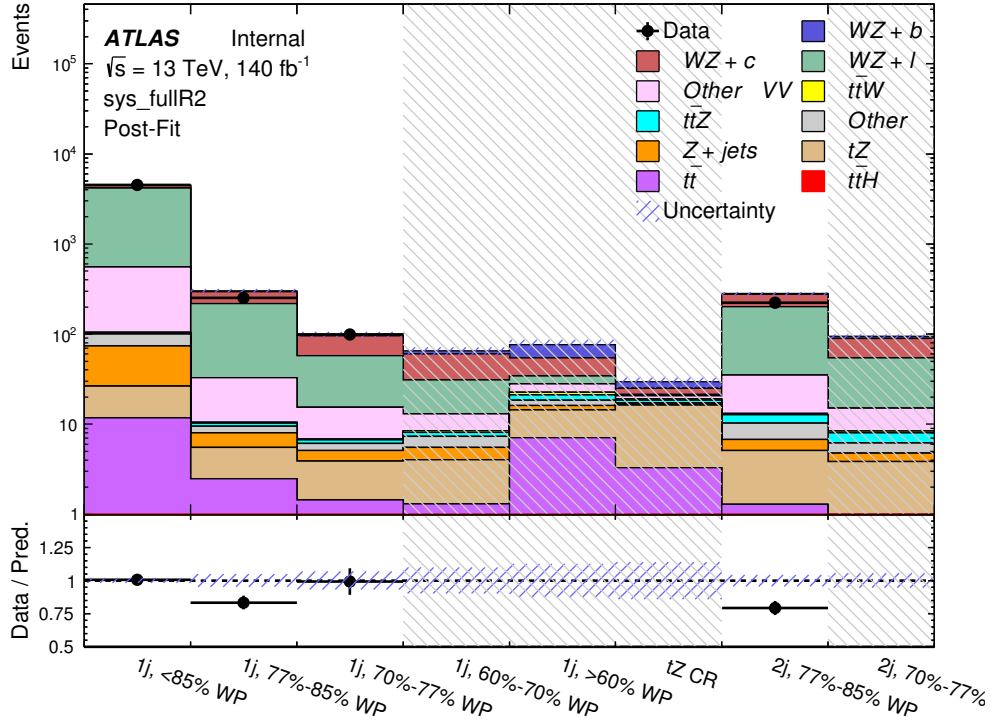
Figure 14: Post-fit summary of fit.

As described in section **??**, there are 226 systematic uncertainties that are considered as NPs in the fit. These NPs are constrained by Gaussian or log-normal probability density functions. The latter are used for normalisation factors to ensure that they are always positive. The expected numbers of signal and background events are functions of the likelihood. The prior for each NP is added as a penalty term, decreasing the likelihood as it is shifted away from its nominal value.

The impact of each systematic uncertainty is calculated by performing the fit with the parameter of interest held fixed, varied from its fitted value by its uncertainty, and calculating $\delta\mu$ relative to the baseline fit. The impact of the most significant systematic uncertainties is summarized in table **??**.

| Uncertainty Source | $\Delta\mu$ | |
|---|---|---|
| WZ + charm cross-section | -0.1966 | 0.2171 |
| tZ cross-section | -0.1521 | 0.1518 |
| WZ + light cross-section | 0.1485 | -0.1411 |
| Other VV + b cross-sction | -0.1115 | 0.1163 |
| Flavor Tagging | 0.0955 | 0.0957 |
| Jet Energy Scale | 0.0613 | 0.081 |
| $t\bar{t}$ cross-section | -0.0662 | 0.0654 |
| Luminosity | -0.0609 | 0.0655 |
| Z + jets cross-section | -0.0284 | 0.0284 |
| Other VV + charm cross-sction | 0.0207 | -0.0202 |
| Muon Trigger Scale Factor | 0.019 | 0.0209 |
| Total Systematic Uncertainty | 0.3511 | 0.3679 |

Table 13: Summary of the most significant sources of systematic uncertainty.

The ranking and impact of those nuisance parameters with the largest contribution to the overall uncertainty is shown in figure **??**.
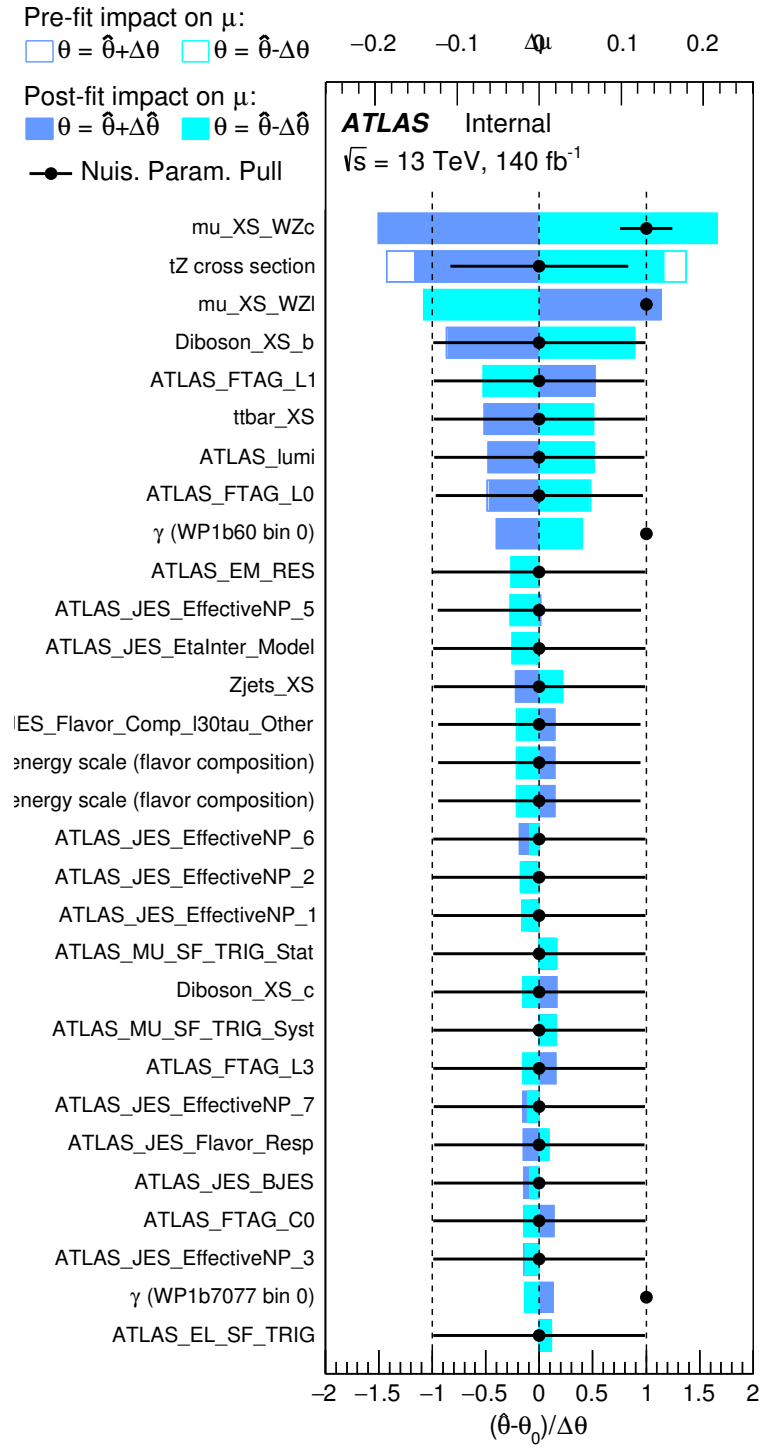
Figure 15: Impact of systematic uncertainties on the signal-strength of $WZ + b$

The large impact of the Jet Energy Scale and Jet Flavor Tagging is unsurprising, as the shape
of the fit regions depends heavily on the modeling of the jets. The other major sources of
uncertainty come from background modelling and cross-section uncertainty. The pie charts in
figure **??** show that for the modelling uncertainties that contribute most correspond to the most
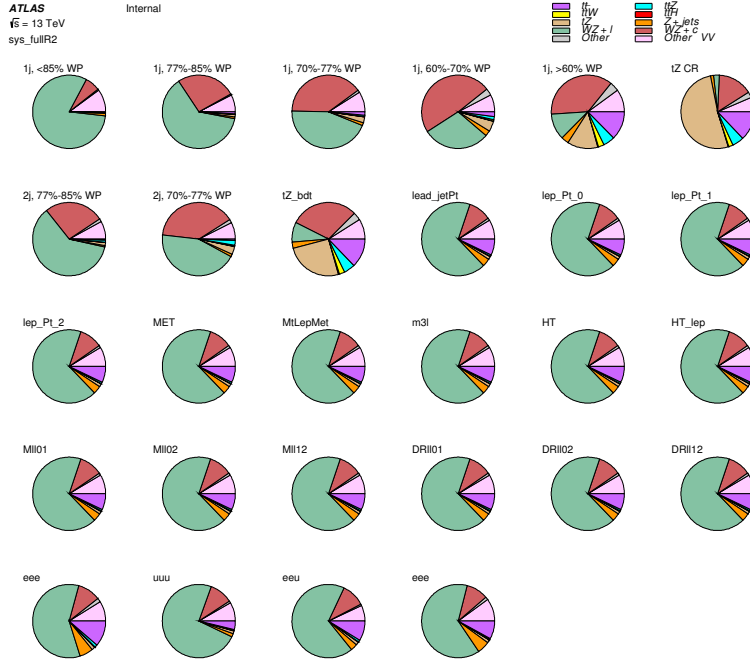significant backgrounds.



Figure 16: Background composition of the fit regions.

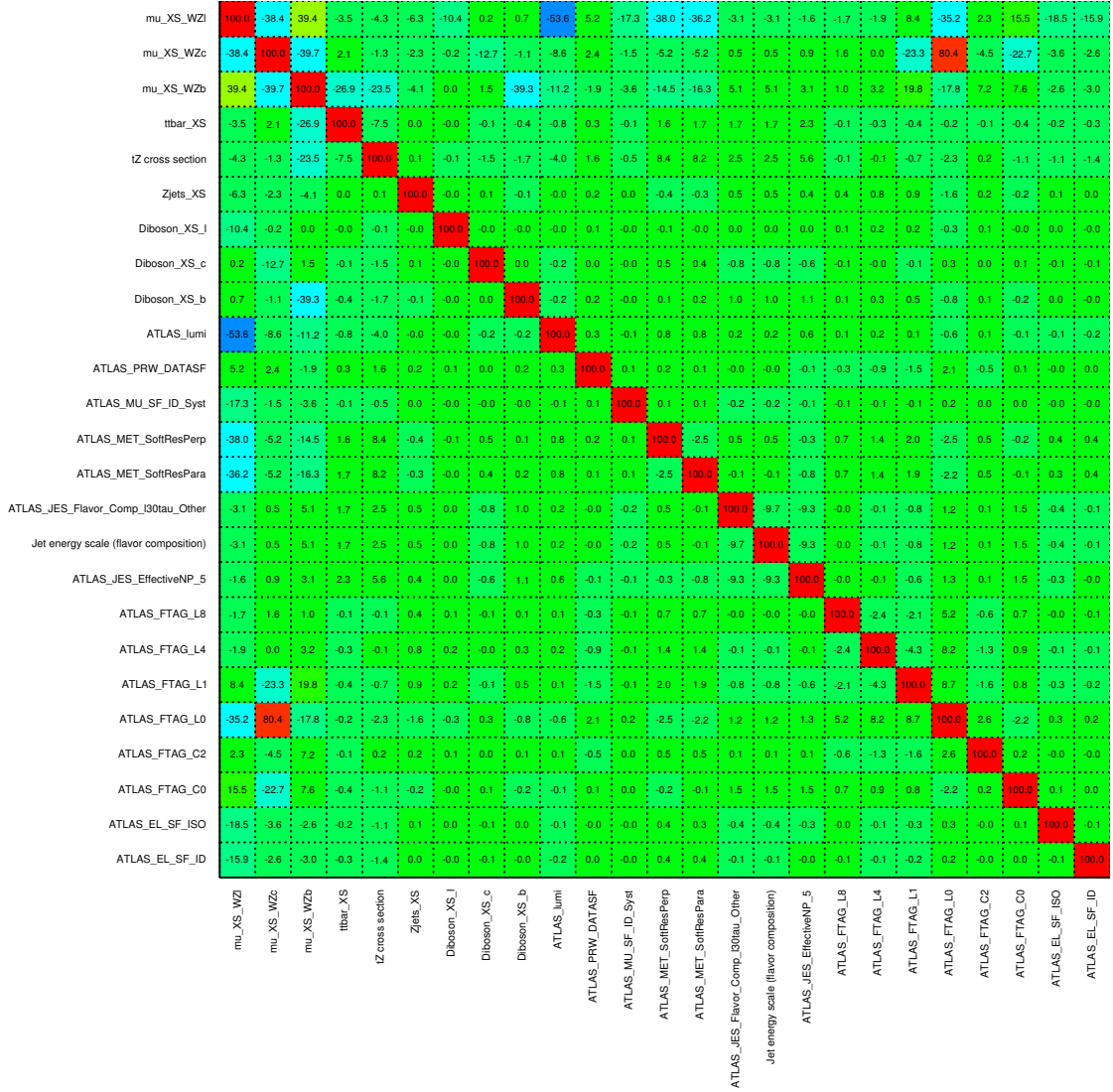The correlations between these nuisance parameters are summarized in figure **??**.

Figure 17: Correlations between nuisance parameters

The negative correlations between $\mu_{WZ+\mathrm{charm}}$ and $\mu_{WZ+\mathrm{b}}$ and $\mu_{WZ+\mathrm{light}}$ are expected: $WZ +$ charm is present in both the $WZ + \mathrm{b}$ and $WZ + \mathrm{light}$ enriched regions, therefore increasing the fraction of charm requires increasing the fraction of $WZ + \mathrm{b}$ and $WZ + \mathrm{light}$. This reasoning also explains the positive correlation between $\mu_{WZ+\mathrm{b}}$ and $\mu_{WZ+\mathrm{light}}$.

Two of the major backgrounds in the region with the highest purity of $WZ + \mathrm{b}$ are tZ and Other $VV + \mathrm{b}$, explaining the negative correlations between $\mu_{WZ+\mathrm{b}}$ and the tZ cross section, and the $VV + \mathrm{b}$ cross section.

The high correlation between the luminosity and $\mu_{WZ+\text{light}}$ arises from the fact that the uncertainty on $\mu_{WZ+\text{light}}$ is very low (around 4%). Small changes in luminosity cause a change in the yield of $WZ$ + light that is large compared to its uncertainty, producing a large correlation between these two parameters.

# 10 Conclusion

A measurement of $WZ$ + heavy flavor is performed using $140 \text{ fb}^{-1}$ of $\sqrt{s} = 13$ TeV proton-proton collision data collected by the ATLAS detector at the LHC. **This section will be include final results once unblinded.**

# References

[1] M. Aaboud et al. 'Observation of electroweak $W^{\pm}Z$ boson pair production in association with two jets in pp collisions at $\sqrt{s} = 13$ TeV with the ATLAS detector'. In: *Phys. Lett.* B793 (2019), pp. 469–492. DOI: 10.1016/j.physletb.2019.05.012. arXiv: 1812.09740 [hep-ex].

[2] T. Gleisberg et al. 'Event generation with SHERPA 1.1'. In: *JHEP* 02 (2009), p. 007. DOI: 10.1088/1126-6708/2009/02/007. arXiv: 0811.4622 [hep-ph].

[3] ATLAS Collaboration. *Electron efficiency measurements with the ATLAS detector using the 2015 LHC proton–proton collision data*. ATLAS-CONF-2016-024. 2016. URL: https://cds.cern.ch/record/2157687.

[4] ATLAS Collaboration. 'Measurement of the muon reconstruction performance of the ATLAS detector using 2011 and 2012 LHC proton–proton collision data'. In: *Eur. Phys. J. C* 74 (2014), p. 3130. DOI: 10.1140/epjc/s10052-014-3130-x. arXiv: 1407.3935 [hep-ex].

[5] *Evidence for the associated production of the Higgs boson and a top quark pair with the ATLAS detector*. Tech. rep. ATLAS-CONF-2017-077. Geneva: CERN, Nov. 2017. URL: https://cds.cern.ch/record/2291405.

[6] ATLAS Collaboration. *Jet Calibration and Systematic Uncertainties for Jets Reconstructed in the ATLAS Detector at $\sqrt{s} = 13$ TeV*. ATL-PHYS-PUB-2015-015. 2015. URL: https://cds.cern.ch/record/2037613.

[7] ATLAS Collaboration. *Selection of jets produced in 13 TeV proton–proton collisions with the ATLAS detector*. ATLAS-CONF-2015-029. 2015. URL: https://cds.cern.ch/record/2037702.

[8] ATLAS Collaboration. 'Performance of pile-up mitigation techniques for jets in pp collisions at $\sqrt{s} = 8$ TeV using the ATLAS detector'. In: *Eur. Phys. J. C* 76 (2016), p. 581. DOI: 10.1140/epjc/s10052-016-4395-z. arXiv: 1510.03823 [hep-ex].

[9] ATLAS Collaboration. *Performance of missing transverse momentum reconstruction with the ATLAS detector in the first proton–proton collisions at $\sqrt{s} = 13$ TeV*. ATL-PHYS-PUB-2015-027. 2015. URL: https://cds.cern.ch/record/2037904.

[10] P. S. A. Hoecker. 'TMVA 4 Toolkit for Multivariate Data Analysis with ROOT'. In: *arXiv:physics/0703039* (2013).

[11] F. Cardillo et al. 'Measurement of the fiducial and differential cross-section of a top quark pair in association with a Z boson at 13 TeV with the ATLAS detector'. In: ATL-COM-PHYS-2019-334 (Apr. 2019). URL: https://cds.cern.ch/record/2672207.

[12] ATLAS Collaboration. 'Luminosity determination in pp collisions at $\sqrt{s} = 7$ TeV using the ATLAS detector at the LHC'. In: *Eur. Phys. J. C* 71 (2011), p. 1630. DOI: 10.1140/epjc/s10052-011-1630-5. arXiv: 1101.2185 [hep-ex].

[13] G. Aad et al. 'Jet energy resolution in proton-proton collisions at $\sqrt{s} = 7$ TeV recorded in 2010 with the ATLAS detector'. In: *The European Physical Journal C* 73.3 (Mar. 2013), p. 2306. ISSN: 1434-6052. DOI: 10.1140/epjc/s10052-013-2306-0. URL: https://doi.org/10.1140/epjc/s10052-013-2306-0.

[14] A. Collaboration. 'Performance of b -jet identification in the ATLAS experiment'. In: *Journal of Instrumentation* 11.04 (2016), P04008. URL: http://stacks.iop.org/1748-0221/11/i=04/a=P04008.